The *J-V* Hysteresis Behavior and Solutions in Perovskite Solar Cells

Meng Wang[1], *Yutian Lei*[1], *Youkui Xu*[1], *Lili Han*[2,*], *Zhipeng Ci*[1,*] and *Zhiwen Jin*[1,*]

Dr. M. Wang, Dr. Y. Lei, Dr. Y. Xu, Prof. Z. Ci, Prof. Z. Jin
[1]Key Laboratory of Special Function Materials and Structure Design (MoE) & National & Local Joint Engineering Laboratory for Optical Conversion Materials and Technology & School of Physical Science and Technology, Lanzhou University, Lanzhou 730000, China

Prof. L. Han
[2]Key Laboratory of Atomic and Molecular Physics & Functional Materials of Gansu Province, College of Physics and Electronic Engineering, Northwest Normal University, Lanzhou 730070, China

E-mail: hanlili@nwnu.edu.cn, cizhp@lzu.edu.cn,jinzw@lzu.edu.cn

Keywords: Hysteresis, factors, origins, strategies, perovskite solar cells

Abstract:

The power conversion efficiency (PCE) of perovskite solar cells (PSCs) has exceeded 25%, showing great potential in the photovoltaic field. However, PSCs often show anomalous current density-voltage (*J-V*) hysteresis behavior in the forward and reverse scanning directions, which makes it impossible to accurately evaluate the performance of PSCs. Therefore, it is necessary to clearly understand the mechanism of hysteresis and suppress the hysteresis. Here, this review mainly focuses on the *J-V* hysteresis behavior in PSCs and strategies to suppress hysteresis: First, we summarize the various factors that affect *J-V* hysteresis in PSCs. And the mechanism behind the various possible origins of hysteresis and the challenges encountered are explored. Then, the strategies to suppress or eliminate the hysteresis are summarized, including optimizing the perovskite light-absorbing layer, improving the performance

This article has been accepted for publication and undergone full peer review but has not been through the copyediting, typesetting, pagination and proofreading process, which may lead to differences between this version and the Version of Record. Please cite this article as doi: 10.1002/solr.202000586

of the carrier transport layer and interface engineering. Finally, wealso provide insights on the future development of the hysteresis.

1. Introduction

Among the third-generation solar cells, perovskite solar cells (PSCs) have achieved rapid development in recent years due to their excellent photovoltaic performance,and low cost fabrication process.[1-5] Since the first reported by Kojima et al. in 2009, the power conversion efficiency (PCE) of PSCs has rapidly increased from 3.8% to more than 25.5%.[6-9] However, PSCs still have some problems that hinder their further development, such as poor long-term stability, the toxicity of lead (Pb) ions and current density-voltage (*J*-*V*) hysteresis.[10-13]

Among them, the *J*-*V* hysteresis is a phenomenon often encountered in PSCs performance testing. The hysteresis makes the efficiency of forward scanning (FS, from short-circuit current to forward bias) and reverse scanning (RS, from forward bias to short-circuit current) of PSCs is overestimated or underestimated, and cannot be accurately characterized performance of PSCs.At present, various level of hysteresis can be generally observed in various types of PSCs such as organic-inorganic hybrid, inorganic, quantum dots and tin (Sn)-based PSCs.[14-18]While, such a common hysteresis has not been observed in solar cells made of other materials (silicon solar cells, dye-sensitized solar cells (DSSCs)).

According to reports, the hysteresis behaviorcan be affected by many factors such as perovskite materials, scanning parameters, composition of carrier transport materials, and device structure.[19,20] These factors can not only affect the level of the hysteresis

but may also change the type of hysteresis.[21] However, we still lack understanding of the mechanism that causes hysteresis. For example, hysteresis may be caused by ferroelectric effect, and may also be caused by ion migration, charge recombination, unbalanced carrier transport or capacitive effect. Although researchers have suggested some possible origins of hysteresis, the exact origin of hysteresis is still under debate.

Meanwhile, hysteresis not only makes the reliability of the efficiency of PSCs are questioned, it is also related to the instability of the device.[22]More serious, the hysteresis issue involves many aspects such as material properties and device physics, and the complex origins of hysteresis and many influencing factors make it extremely difficult to eliminate the hysteresis. Therefore, this is an urgent problem to be solved. Fortunately, many strategies have been proposed in recent years to suppress or eliminate the hysteresis.[23] These strategies are contributed to accurately assess the efficiency of the PSCs and promote the further research of PSCs. Meanwhile, some researchers have also summarized the origin and basic understanding of the hysteresis behavior of PSCs.[24] They summarized the excellent research results on hysteresis very well, and enhanced the understanding of hysteresis for related researchers. But our understanding of hysteresis is still insufficient, and there is a lack of systematic research on the hysteresis.

This review mainly discusses the factors that affect the hysteresis, the mechanisms behind various possible origins and the methods to solve the hysteresis. First, many factors that affect hysteresis from different perspectives are discussed. Next, we discuss how the various possible origins cause the hysteresis, and put forward some of the

challenges encountered by these views. The strategies to suppress or even eliminate the hysteresis are further introduced in detail, including optimizing the perovskite light-absorbing layer, improving the performance of the carrier transport layer and interface engineering. Finally, we put forward some problems that still exists in *J-V* hysteresisand provided insights into the future development of the hysteresis.

2. PSCs and Hysteresis

2.1 Structure and Composition of Perovskite

The general structural formula of perovskite is ABX_3, where A is a monovalent cation, which can be organic cations such as methylammonium (MA^+, $CH_3NH_3^+$), formamidinium (FA^+, $HC(NH_2)_2^+$), or inorganic cations cesium (Cs^+) and rubidium (Rb^+);[25] B is divalent metal cation, commonly used are Pb^{2+}, Sn^{2+}[26]; X is a halogen anion, including iodine (I^-), bromine (Br^-) andchlorine (Cl^-). In the cubic crystal structure of ABX_3 perovskite, where A cation are located at the eight corners of the cubic unit cell, B cation are located at the center, and X anion are located at the center of the six faces. And B cation and X anion form an octahedron with $[BX_6]^{4-}$ arrangement.

The difference in chemical composition will affect the crystal structure. The stability of the perovskite structure can be predicted by the Goldschmidt tolerance factor (as shown in Equation 1):[27]

$$t = \frac{r_A + r_X}{\sqrt{2}(r_B + r_X)} \qquad (1)$$

Where r_A, $r_B$and $r_X$are the radius of the A, B and X ions respectively. When *t* is between 0.8 and 1, the perovskite structure is often formed. And the radius of the A cation is too

large (t>1) or small (t<0.8) can cause lattice distortion and make the perovskite structure unstable.

2.2 Device Architectures

At present, PSCs can be roughly divided into the following sixstructures according to the structure and position of the electron transport layer (ETL): mesoporous, super-mesoporous,planar n-i-p (regular), planar p-i-n (inverted), bi-layer and ETL-free structure as shown in the **Figure 1**.

Mesoporous and super-mesoporous structures are generally used as scaffolds to support perovskites, which can facilitate the nucleation and growth, inhibit the formation of pinholes, and also play a role in blocking holes. At present, the devices with mesoporous structures have higher PCE, mainly because the mesoporous structure can increase the light-receiving area of the perovskite light-absorbing layer. In the mesoporous PSCs, the electron transport material (ETM) is metal oxide with a lower energy level than perovskite, such as titanium dioxide (TiO_2) and zinc oxide (ZnO). The electrons can be transferred by these mesoporous structures, and there is a larger contact area between ETL and the perovskite layer, which can greatly promote the process of electron extraction and transfer.Different from the mesoporous PSCs, the super-mesoporous PSCsuse mesoporous insulatedscaffold. The materials are generally aluminium oxide (Al_2O_3) and zirconium dioxide (ZrO_2) with higher conduction band energy levels.[28] The electrons generated in the perovskite layer cannot be transferred through the mesoporous insulatedscaffold. It is delivered through the perovskite material itself.[29,30] This is mainly because Al_2O_3 as an insulator cannot transport

electrons, and as mesoporous scaffold supporting the perovskite helps to form continuous perovskite structure.[28,31] The perovskite itself can transport carriers (electrons and holes), so the generated electrons can be directly transferred from the perovskite to the conductive substrate.

The PSCs with planar structure can be divided into n-i-p structure and p-i-n structure according to the different positions of hole transport layer (HTL) and ETL. Generally speaking, the PCE of the inverted structure PSCsis lower than that of the normal structure.[32]This is mainly ascribed to the poor properties of commonly used [6,6]-phenyl-C_{61}-butyric acid methyl ester ($PC_{61}BM$) materials.For example, $PC_{61}BM$ has problems such as low coverage and electron mobility, interface recombination, and easy degradation in ambient air.[33-35] This will affect the photovoltaic performance of the inverted device.Planar structures are easier to prepare than mesoporous structures, and can be prepared by low-temperature solution processes (less than 100°C) and vapor deposition methods. However, because the small contact area with the perovskite layer and low carrier transport rate, the efficiency of the planar PSCs is generally lower than that of the mesoporous structure. And when SnO_2 or TiO_2 is used as ETL, the level of the hysteresis of the planar PSCs is often greater than that of the mesoporous structure.[36,37]This may be due to the more balanced and faster carrier transport of PSCs with mesoporous structure. The carrier transport layer of the bi-layer PSCs is composed of two materials. For example, the step jumping makes electrons easier to be transported and reducing the energy barrier for electron transport in the common $PC_{61}BM/C_{60}ETL$.[38] And in order to avoid the troubles of ETL, ETL-free PSCs have

also received attention.

2.3 Basic Working Mechanism of PSCs

The working mechanism of PSCs is roughly as follows: sunlight passes through the transparent substrate and irradiates the perovskite layer, and the incident light is absorbed by the perovskite layer to generate electron-hole pairs. These electrons and holes are separated and then transported through ETL and HTL, respectively. Then the electrons travel along the external circuit to the metal electrode, where the current is collected to complete the entire photoelectric conversion process. One of the most important steps is to ensure that electrons and holes can be separated smoothly to reach the electrode through ETL and HTL, which requires the energy levels of the perovskite material to match the ETM and hole transport material (HTM).The energy level diagram of typical materials is shown in the **Figure 2a**. Generally, the minimum energy level of the conduction band (the lowest molecular unoccupied orbital (LUMO) energy level) of ETM needs to be smaller than that of perovskite materials, while the maximum value of the valence band energy level (the highest molecular occupied orbital (HOMO) energy level) of HTM needs to be greater than the perovskite material. When the energy level difference is too small (the LUMO energy level of the ETM is too large or the HOMO energy level of the HTM is too small) or the energy level does not match (the electrons encounter greater energy potential barrier during the movement) will hinder the separation and extraction of electrons or holes, and ultimately affect the performance of the device. It can be seen that suitable materials should be selected when preparing the devices to ensure energy level matching and obtain excellent

performance.

2.4 Hysteresis Index

It is necessary to understand the types of hysteresis and how to measure the level of hysteresis for us. According to the *J-V* curve obtained by the FS and RS, the hysteresis can be divided into three categories: normal hysteresis, hysteresis-free and inverted hysteresis, as shown in **Figure2b**.[39] Normally, the normal hysteresis refers to the open-circuit voltage (V_{OC}), and the fill factor (FF) or photo-generated currentof the RS is higher than the FS (resulting in higher photovoltaicperformance), while the inverted hysteresis is the opposite. Specially, the RS curve intersect withFS curve at a point, which is called mixed hysteresis (normal hysteresis and inverted hysteresis exist at the same time). These hysteresis phenomena are affected by many factors, such as scan rate and perovskite material type.

In order to roughly measure the level of hysteresis, we need to introduce the concept of hysteresis index (*HI*). The *HI* can be calculated by Equation 2:[40]

$$HI = \frac{PCE_{RS} - PCE_{FS}}{PCE_{RS}} \qquad (2)$$

Where PCE_{RS} and PCE_{FS} represent PCE measured under RS and FS, respectively.The more positive value of the *HI* means more serious normal hysteresis and vice versa.When the value is very close to zero that means no hysteresis.Although *HI* cannot accurately measure the level of hysteresis, and has even been seriously questioned,[41] it can still be used as a test method to estimate the level of hysteresis at this stage.

3. Influencing Factors of Hysteresis

In the past numerous studies of hysteresis in PSCs, researchers have found that the existence of hysteresis is affected by multiple factors. These factors may come from the perovskite material itself, or from external test conditions and the environment. Understanding the influence of these factors on hysteresis can help us choose the appropriate method to suppressthe hysteresis. In this section, we will carefully discuss the influence of these factors on the hysteresis from both internal and external factors.

3.1 Internal Factors

3.1.1 The Influenceof Materials

Each functional material of the device affects the hysteresis in different ways. First, the material of the perovskite light-absorbing layer hasparticularly significant effect on the hysteresis. In $APbX_3$ structure, different element composition will cause different hysteresis. For example, Qiang et al. found the hysteresis of $MAPbI_3$-based is greater than $FA_{0.15}MA_{0.85}PbI_3$-based PSCs in the common FTO/compact TiO_2(c-TiO_2) /perovskite/2,2′,7,7′-tetrakis[N,N-di-p-methoxyphenylamine]-9,9′-spirobifluorene (Spiro-OMeTAD)/Ag structure.[42]This can be attributed to the doping of an appropriate amount of FA ions which improves the purity and grain size of the crystal.Another study also confirmed the effect of A-site elemental composition on the hysteresis.[43] At the same time, the composition of the elements at the X-site also has certain influence on the hysteresis. Compared with pure I halide perovskite, the presence of Cl or Br ions can show lower hysteresis.[44]In general, a relatively large

grain size (fewer defects) helps to reduce the hysteresis and increase the efficiency.[45] However, the *HI* measured by Moshaii et al. in $MAPbI_3$-based PSCs with grain sizes of 300, 200, 100, and 50 nm are 0.33, 0.28, 0.19, and 0.12, respectively (the *J-V* curve as shown in the **Figure3a-d**).[46]This indicates that the hysteresisdecreases as the grain size decreases. This can be ascribed to the fact that the small grain size reduces the ion accumulation between the perovskite layer and the carrier transport layer (**Figure 3e**), resulting in smaller low-frequency capacitance and lower hysteresis. But no matter what, the grain size of the perovskite can indeed significantly affect the hysteresis.Similarly, we need to pay attention to the influence of thickness of the perovskite layer on the hysteresis. In the $PC_{61}BM$-based PSCs, the *HI*values of $MAPbI_3$perovskite layers with thicknesses of 150, 300, 600, and 800 nm are 0.40, 0.27, 0.10, and 0.08, respectively.[47]This indicates that the hysteresis decreases as the thickness of the perovskite layer increases. In the planar heterojunction PSCs ($MAPbI_{3-x}Cl_x$-based), the opposite effect is shown.[48] It can be seen that the proper composition, the grain size of perovskite and thickness of the perovskite layer are critical to hysteresis of the PSCs.

Further, the thickness of ETL has a huge effect on the hysteresis. As shown in the **Figure3f-i**, the thickness of mesoporousTiO_2(mp-TiO_2)layer shows different level of hysteresis at 0 (planar), 100, 200, and 350 nm.[49] Other studies have also confirmed the effect of mp-TiO_2 thickness on the hysteresis.[50,51]The study also found that the *HI* of the device increases as the size of the mp-TiO_2 nanoparticles increases, which indicates that the crystal size of the ETM may also have an effect onhysteresis.[52]In addition, the

ETM also has significant effect on hysteresis. Taking tin dioxide (SnO_2) and TiO_2 as ETL respectively, it is found that SnO_2 devices exhibit lower hysteresis than typical TiO_2 devices.[53]Research by Namkoong et al. also confirmed the effect of ETM on the hysteresis.[54] Therefore, selecting the appropriate ETM, appropriate thickness and crystal size can improve the hysteresis of PSCs.

Likewise, the HTM will also affect the hysteresis behavior. Jung et al. compared two different HTMcopper cobalite ($CuCo_2O_4$) and nickel(II) oxide (NiO_x) in planar PSCs.[55] The *HI* are 0.003 and 0.011, respectively. It is confirmed that $CuCo_2O_4$ has stronger inhibitory effect on the hysteresis behavior of planar PSCs than NiO_x. In some cases, there areHTL-free in PSCs.Rao et al. compared the hysteresis behavior with or without HTL, and found that CuS nanoparticles (NPs) are used as HTM, they exhibit smaller hysteresis than when there is HTL-free.[56]In addition, different electrode materials may also affect the hysteresis behavior.[57] At the same time, it is necessary to pay attention to the energy level matching when selecting these functional materials. Otherwise, the separation and extraction of electrons and holes will be unbalanced, which can affect the hysteresis. These results provide us with some new perspectives on suppressthe hysteresis.

3.1.2 The Influence of Device Architecture

Different device architectures not only affect the main performance parameters such as PCE and FF, but also affect the hysteresis of the device, which has received extensive attention in recent years. When TiO_2 or SnO_2 is used as ETL, the hysteresis of the mesoporous PSCsare usually less than that of the planar structure. This is mainly

due to the large contact area between the mesoporous ETL and the perovskite layer, which promotes the electron transport process.[49,58-61]Comparison of the *HI* values and photovoltaic performance of PSCs with planar and mesoporous structures are listed in **Table 1**. Similarly, because the Al_2O_3 used in the super-mesoporous PSCs is an insulating scaffold and lacks the existence of compact TiO_2 layer, electron transport can only be completed by the perovskite itself, finally result in slower charge separation and transport rate. Therefore, the super-mesoporous structure PSCs shows more serious hysteresis than the mesoporous structure. In the planar structure, the hysteresis can be adjusted by applying the inverted p-i-n structure when the normal n-i-p structure has a severe hysteresis.For example, the conductivities of common carrier transport materials Spiro-OMeTAD, poly[bis(4-phenyl) (2,4,6-trimethylphenyl)amine](PTAA):tert-butylpyrridine(tBP) + lithium-bis(trifluoromethanesulfonyl)-imide (Li-TFSI), Poly(3,4-ethylenedioxythiophene):poly(styrenesulfonate) (PEDOT:PSS), $PC_{61}BM$, and TiO_2 are 0.01, 0.034, 0.014, 0.016, and 0.00006 $mS \cdot cm^{-1}$, respectively.[62]While the conductivity of $MAPbI_3$ is 0.015 $mS \cdot cm^{-1}$. After the FTO/TiO_2/$MAPbI_3$/PTAA (or Spiro-OMeTAD)/Au structure is converted to ITO/PEDOT:PSS/$MAPbI_3$/$PC_{61}BM$/Au, the carrier transport rate tends to be more balanced and makes the inverted structure exhibit the relatively small hysteresis.[62]In the bi-layer structure, the bi-layer ETM promotes effective charge separation and reduces the charge accumulation at the ETL/perovskite interface. Therefore, the hysteresis is smaller compared with the single-ETL PSCs. For example, the *HI* of TiO_2@SnO_2-based and SnO_2-based PSCs are

0.015 and 0.195, respectively.[63]The bi-layer structure greatly reduces the hysteresis of the device, mainly because it reduces the charge recombination and promotes the extraction of electron. In summary, we should select suitable device architecture to reduce the hysteresis when preparing the device.

3.2 External Factors

The internal factors are mainly caused by the selected materials and some basic properties of the materials, while the external factors are mainly determined by the parameter setting and environment during the test. The external factors can be controlled artificially to achieve an ideal result.

3.2.1 Influence of Device Test Conditions

The study found that the scan rate, bias voltage and precondition during the test can affect the hysteresis behavior of PSCs. **Figure 4** shows the effect of bias voltage and scan rate on the hysteresis.[64] The scan rates not only affects the level of the hysteresis, but also the type of hysteresis.For the mesoporous TiO_2-based $MAPbI_3$PSCs, the hysteresis increases with the continuous increase of the scan rates in the low range (<1000mV/s).[65] There is almost no hysteresis when the scan rate is extremely low. The hysteresis decreases as the scan rate increases when the scan rate is high (greater than 10000 mV/s), and it may even appear as an inverted hysteresis.The PSCs with ITO/$NiCo_2O_4$(nickel cobalt oxide)/$MAPbI_3$/$PC_{61}BM$/bis-C_{60}/Ag structure showed the opposite situation.[66]As the scan rate increased (less than 500 mV/s), the hysteresis significantly decreased. These results indicate that the hysteresis behavior of PSC is

related to scan rate and structure.

Different start bias voltagesand bias voltage range can also cause changes in the hysteresis. When scanning from a more negative bias voltage, it can increase the hysteresis of PSCs.[67]In inverted $MAPbI_3$-based devices, the level and type of hysteresis will vary with the variation of the bias voltage range.[64] This may be related to ion migration, especially when the bias voltage is greater than the V_{OC}, additional polarization will be generated. In addition, setting an external bias voltage (pre-poling) before the test can also affect the hysteresis.Jiang et al. studied the influence of different precondition on the hysteresis.[68] The *HI*values (inverted hysteresis) under 0, 0.5 and -0.5V bias voltages are 0.003, 0.007 and 0.046, respectively. This result is attributed to ion migration and accumulation induced by external electric fields in different directions. At the same time, the type of hysteresis can also change with the pre-poling biasvoltage, and even mixed hysteresis can occur.[21]

Voltage settling time (waiting period to measure current after applying a given voltage)can also affects the hysteresis. The study found that the hysteresis was alleviated as the voltage stabilization time increased from 200 ms to 3000 ms for mesoporous TiO_2-based PSCs.[50]Meanwhile, as the number of scans increases (forward scan and reverse scan alternately), not only PCE canbe improved but the hysteresis can be alleviated.[69] The temperature during the test may also affect the hysteresis behavior.[70] The influence of test conditions on hysteresis may be related to the internal electric field, ion migration process, device structure and ferroelectric polarization, which further increases the complexity of analyzing the origin of

hysteresis.

3.2.2 LightSoaking

The light soaking effect can be used to improve the photovoltaic performance of DSSCs.[71] The structure of PSCs is similar to DSSCs, so the light soaking effect may affect the photovoltaic performance of PSCs. Current evidence indicates that light soaking before the test can increase the V_{OC} and FF of the device, the short-circuit current (J_{SC}) is slightly reduced, finally the PCE of device is increased.[72]In TiO_2-based PSCs, light soaking can increase the oxygen vacancies in the ETL and charge extraction is promoted, thereby improve the efficiency of device.[73,74]However, the light soaking effect is usually reversible, reflecting the light soaking instability of the device.Moreover, long-term light soaking may cause performance degradation.[75] The light soaking effect not only affects the PCE of planar PSCs, but also affects the level and type of hysteresis.[49] This is mainly because light soaking reduces the defect density in the perovskite and defect-assisted recombination. During the light soaking process, the defect state of the interface may be passivated, reduces the charge recombination and promotes carrier transport at the perovskite/carrier transport layer interface.[76] It should be noted that the degree of influence of the light soaking effect on the hysteresis varies with the ETL and the material of the intermediate layer.[77]

4. Origins of Hysteresis

Although the exact origin of hysteresis is still under debate, studies have found that possible origins of hysteresis include as follows: ferroelectric effect of materials,

unbalanced carrier transport, capacitive effect, ion migration and charge recombination. The anomalous hysteresis in PSCs may be caused by one or more origins. In this section, we will introduce how these possible origins cause the hysteresis in detail.

4.1 Ferroelectric Effect

The ferroelectric effect can not only enhance the photovoltaic performance of the device, but also cause the *J-V* hysteresis. But, whether or not the hybrid perovskite (especially for $MAPbI_3$) is ferroelectric is highly controversial.Some studies believe the hysteresis caused by the ferroelectric effect is generally common in organic-inorganic hybrid PSCs compared with other types of PSCs.Inthis regard, through piezoelectric force microscopy (PFM), standard polarization-electric field (P-E) loops, Raman spectroscopy and Fourier transform infrared spectroscopy (FTIR), the research found that organic-inorganic hybrid perovskite ($MAPbX_3$) has ferroelectric polarization characteristics and slow polarization may occur.[78]However, some studies have put forward different opinions on whether hybrid perovskite (especially for $MAPbI_3$) is ferroelectric. For example, Ovchinnikova and Abate conducted a lot of experimental work and the results showed that $MAPbI_3$ is not ferroelectric.[79,80]Nevertheless, as a possible origin of hysteresis, discussions are still needed to promote the understanding of hysteresis.

The hysteresis caused by the ferroelectric effect is discussed as follows: There is an intrinsic built-in electric field in the perovskite layer, and the energy band diagram of PSCs with n-i-p structure without an external electric field is shown in **Figure**

5a.[81]In addition, E_p (ferroelectric polarization field) can be used as another driving force for charge separation or recombination. The widths of the depletion region on both sides becomes (W_{bi-1}-W_{p-1}) and (W_{bi-2}-W_{p-2}) when negative poling (**Figure 5b**). The depletion region becomes narrower and the driving force for charge separation decreases, which is not conducive to the transfer and collection of carriers. Therefore, the photovoltaic performance of the device is impaired.The polarization field direction caused by ferroelectric polarization is consistent with the built-in electric field in positive poling condition (**Figure 5c**). The widths of the depletion region on both sides is increased, which correspondingly increases the driving force for charge separation, thereby enhancing the photovoltaic performance of the device. Based on this, the RS (positive poling) has a higher PCE, which in turn causes the hysteresis between FS and RS in the *J-V* curve.

When there is no external electric field, the perovskitecan undergo multi-directional spontaneous polarization due to its ferroelectricity. Moreover, the light-induced polarization is not strong, and the polarization direction of the ferroelectric domains in the perovskite material is disorderly. Different scanning directions can change the polarization direction under applied electric field, which helps to understand why the scanning direction affects the hysteresis. Specially, the ferroelectric effect in PSCs can also explain why the hysteresis of mesoporous TiO_2-based PSCs is smaller than that of planar heterojunction PSCs and super-mesoporous Al_2O_3-based PSCs.[82]In addition, the ferroelectric effect helps to understand why the scan rate and bias voltage affect the hysteresis behavior.[67] The

ferroelectric effect can explain some hysteresis behavior, but it does not represent the exact origin of hysteresis in PSCs. For example, $CsPbI_3$ cannot become a ferroelectric at room temperature, so the ferroelectric effect cannot be used to explain the hysteresis in $CsPbI_3$-based PSCs.[83] Some studies have also shown that the time scale of MA dipole reorientation is much smaller than the related process of *J-V* hysteresis.[84] Therefore, the impact of other origins on hysteresis needs to be considered.

4.2 Unbalanced Carrier Transport

The unbalance of carrier transport is considered to be one of the important origins of hysteresis. Studies have found that the halide perovskite has ambipolar nature, which can transport electrons and holes by itself.[85] But the separation rate of holes is higher than that of electrons due to the difference in effective diffusion length.Studies have shown that the unbalance of carrier extraction can lead to the charge accumulation at the interface, which in turn causes the hysteresis. The existence of ETL helps to extract and collect electrons, alleviate the problem of the unbalance of carrier transport rate in the perovskite layer, and can also reduce the accumulation of space charges at the interface to inhibit the hysteresis. The above points are helpful to understand why the hysteresis of super-mesoporous structure and regular planar structure are more serious than the mesoporous PSCs, because the mesoporous structure can extract electrons more effectively.

However, because of the unbalance of the carrier transport rate in ETL and HTL, there is still an unbalanced carrier transport phenomenon in PSCs. For example, the

electron mobility of the TiO_2ETL (10^{-4} $cm^2 \cdot V^{-1} \cdot s^{-1}$) is lower than the hole mobility of some common HTL (Spiro-OMeTAD, PTAA). The level of hysteresis can be reduced by improve the carrier mobility of ETL and/or HTL, which can also explain why different ETL and HTL cause different level of hysteresis.[86]In addition, some electrons can remain in the ETL and perovskite layer cause capacitance and affect hysteresis due to the unbalanced carrier transport. The above analysis shows that the purpose of reducing or eliminating hysteresis can be achieved by optimizing the carrier transport process.

4.3 Charge Recombination

The charge recombination is considered to be another important origin of the hysteresis. There are numerous defects at the interface between the perovskite light-absorbing layer and the carrier transport layer and the bulk grain boundaries (GBs) of the perovskite. These bulk and interface defects can be used as traps for trapping electrons and holes, resulting in non-radiative recombination and affecting the device performance.[87]The trapsare filled under forward-biased working conditions to produce good interface contact; it is emptied and release the trapped charge carriers under short-circuit conditions, resulting in poor operation until the next trapping process. In the above process, the carriers first recombine at the traps and then the photocurrent gradually increases. Therefore, the traps filling process will cause the photocurrent saturation time to be delayed, and the photocurrent can slowly decay under short-circuit conditions. The same is true of photovoltage changes. Therefore, the photocurrent and photovoltage are delayed by the charge

trapping-detrapping process.

The density of defects at the GBs and interfaces of the perovskite layer is relatively high, and there are a lot of traps. The trap states are shallow or deep, and the deep trap states can cause charge accumulation and recombination, which will adversely affect the charge extraction efficiency and slow down the photoelectric response of the device. Meanwhile, it can cause certain energy loss, reduce the photovoltaic performance and increase the hysteresis of PSCs.[88]Therefore, it is necessary to reduce the trap density and charge recombination by preparationof high-quality perovskite films or interface treatment, so as achieving the purpose of suppressthe hysteresis. For example, the introduction of potassium thiocyanate (KSCN) improves the crystallinity of perovskite, and perovskite film with large grain size and few GBs is obtained.[89] It reduces the trap density and promotes charge transfer, and significantly reduces the hysteresis level of the device.In addition, the annealing temperature of some ETLs can affect the trap density, and thus exhibit different levels of hysteresis. The **Figure 5d**shows the relationship between the annealing temperature of the SnO_xETL and the *HI*, which is attributed to the change of trap state leading to a better Fermi level arrangement (**Figure 5e**).[88] The above examples all show that reducing defects can effectively suppress hysteresis, indicating that charge recombination is likely to cause hysteresis.

4.4 Ion Migration

Perovskite materialsare considered to be a kind of ionic crystal with the ion conductive properties.[90] As shown in the **Figure6a**, point defects and GBs in the film

provide pathways for ion migration.[91] Therefore, some ions and vacancy defects in the perovskite can migrate under the action of an external electric field. And the existence of ion migration was confirmed by photo-thermal induced resonance (PTIR)microscopy, time-of-flight secondary ion mass spectrometry (ToF-SIMS) and temperature-dependent impedance spectroscopy.[92-95]Ion migration is considered to be an inherent characteristic of perovskite, which not only causes the unbalanced element distribution and unstable structure in the light-absorbing layer, but also a possible origin of the hysteresis that cannot be ignored.[96,97]

Take typical $MAPbI_3$-based PSCs as an example, the ion species that can migrate include interstitial iodide ions (I_i), I^-, $Pb^{2+}$and MA^+ and the corresponding vacancies (V_I, V_{MA}, V_{Pb}). The study also found the existence of interstitial hydrogen migration.[98]These ions can migrate through grains and GBs, and can even move at the interface.[68] Under different bias conditions, the above ions and vacancies will move to the corresponding interfaces on both sides in different directions.In order to maintain the electrical neutrality of the film, the positive ions or vacancies accumulated at the interface attract electrons to cause n-type doping.[99]P-type doping is formed at the interface on the other side. In addition, charge accumulation at the interface caused by ion migration leads to the band bending and the interface energy barrier changes, which affects the transport of carriers and ultimately affects the photovoltaicperformance of PSCs.As shown in the **Figure6b**, it explains how ion migration causes hysteresis.[100]The inherent built-in electric field can drive the ions to undergo directional movement, forming a local electric field that can partially offset

the built-in electric field. Ions and vacancies further migrate under reverse bias, which enhances the shielding of the built-in electric field and hinders the extraction of charge carriers; the local electric field decreases or even disappears under forward bias, which is beneficial to extraction of carriers. Therefore, the degree of influence on ion migration is different under different working conditions, and the hysteresis behavior is formed.

The activation energy can be used to measure the migration ability of ions. Moreover,the activation energy can be used to determine which type of ion migration mainly causes the hysteresis in PSCs. The migration pathways of I^-, MA^+ and Pb^{2+} as shown in the **Figure 6c**. The corresponding theoretical activation energies are calculated according to the first principles, and the values of I^-, MA^+ and Pb^{2+} are 0.58 eV, 0.84 eV and 2.31 eV respectively.[100]Among them, the activation energy of hysteresis (0.60-0.68eV) and$I^-$are relatively close, so I^-migration may be the origin of hysteresis.[100] In addition, the activation energies of V_I, V_{MA}, V_{Pb} and I_i are 0.08 eV, 0.46 eV, 0.80 eV and 0.08 eV, respectively.[101]**Figure 6d-g** show the migration pathways of V_I, V_{MA}, V_{Pb} and I_i. This confirmed that V_I and I_i migrate easily in the film. But the speed ofmigration is too fast (<1μs) to explain the hysteresis behavior (millisecond level).[101] The slow response caused by V_{MA} and V_{Pb} migration can be used to explain the hysteresis in PSCs.

Furthermore, the hysteretic MA^+ and I^- migration can be observed by tr-ToF-SIMS technology.[102] The ion migration caused by the bias under light will cause the residual current to last more than 200 s, and the residual current can be

ignored under the condition of no light. And it is found that MA^+ migration will contributes to the current-voltage hysteresis related to illumination. Interestingly, ion migration is also related to the degradation of PSCs.[103]Therefore, inhibit the ions and vacancies migration are particularly important to improve the performance of PSCs. It can suppress ion migration by reducing defects in the film, controlling crystallization, surface treatment, and using additives to achieve the purpose of improve performance and suppressthe hysteresis.

4.5 CapacitiveEffect

Ferroelectricity, dipolar polarization, trap states, and electrode polarization may all cause capacitance in PSCs.[104]For example, the space charge accumulated at the interface traps can cause capacitance. In addition, ion migration and unbalanced carrier transport can cause a large amount of ions and charges to accumulate at the interface. The accumulated ions and charges will cause the electrode to be polarized, resulting in capacitive effect.[105]Generally, capacitance can be chemical or dielectric, including contact and bulk capacitance. In addition, Almora et al. found that the low-frequency capacitance value has nothing to do with the thickness of the perovskite film, which indicates that the capacitance is related to the interface properties.[104]Meanwhile, the photo-induced giant dielectric constant can be observed at low frequency.[104,106]The photocurrent can be divided into steady-state current (J_0) and non-steady-state current ($J_{n(t)}$) in PSCs. The J_0 is related to the extraction and recombination of charge carriers, while the latter is related to the capacitive effect are confirmed by impedance spectroscopy, stepwise scanning and dynamic J_{SC}transient

process.[105]As shown in the **Figure7a**, three arc characteristics of low, medium and high frequency can be clearly identified in the impedance spectroscopy.[107]Among them, the medium-frequency arcs is related to chemical capacitance, and high-frequency arcs is related to selective contact. The low frequency arc seems to be related to the dielectric relaxation process, and the slow dielectric relaxation can be attributed to the electrode polarization.[106,107]The slow decay process of low-frequency capacitance and capacitive current related to electrode polarization can cause *J*-*V* hysteresis.

The study found that different step interval times can cause different levels of hysteresis (**Figure 7b,c**).[105]Due to the slow decay of the capacitive current, the capacitive effect can affect the current of the device under different scanning directions and scanning rates. When the step interval time is short (i.e. fast scan rate), there will still be a part of the residual capacitive current at the end of each step, and the sign of the current is related to the scan direction (**Figure 7d**).[105]The negative capacitive current can cause the photocurrent to be less than the J_0 under FS condition; the positive capacitance current can cause the photocurrent to be greater than the J_0 under RS condition.Therefore, there is a significant difference between the FS and RS which result in *J*-*V* hysteresis.But the capacitive hysteresis will not become more serious as the scan rate continues to increase. As shown in the **Figure7e**, the capacitance will decrease sharply and the capacitive current can also decrease when the scan rate is extremely high, thereby suppress this capacitive hysteresis.[105] The above analysis is how the capacitive effect causes hysteresis, and helps to understand

why the scan rate affects the hysteresis.

The *J-V*hysteresis is related to the scanning direction and the voltage settling time (the photocurrent is preferentially stored as capacitive charge at the FS, and the stored charge is released at the RS).[50] The former determines the accumulation and release of capacitive charge, while the latter determines the amount of accumulation and release. The capacitive effect can also understand why the perovskite crystal size and device structure affect the hysteresis. Because the large crystal size and the existence of the mesoporous structure can reduce the low-frequency capacitance related to hysteresis.[50]

4.6 Discussion on the Origins of Hysteresis

Although current research has proposed some origins of hysteresis, the exact origin of hysteresis is still uncertain. The *J-V* hysteresis may be a complicated process caused by multiple origins rather than a single origin. Some studies in recent years have also shown this view.[108]Recently, some other origins have been discovered. For example, Segawa et al. found that the tunneling phenomenon may be a new origin.[109]

Some studies have also questioned these possibleorigins. Studies have found that hysteresis occurs on the time scale of milliseconds to seconds.[110]Therefore, it can be judged from the time scale whether it is the origin of hysteresis. The MA ion dynamics study shows that the ferroelectric domain wall can pass through the device in about 0.1-1ms, which is significantly faster than the hysteresis response time.[111]The study also found that the charge trapping process takes place faster than

the hysteresis.[112] However, the charge trapping and detrapping time may be related to the device structure and processing method, thus exhibiting different time scales. At the same time, Chen et al. found that it takes several minutes for moving ions to achieve slow redistribution, which is significantly slower than hysteresis.[105] Therefore, a lot of work remains to be done to determine the exact origin of the hysteresis.

5. Method of reducing or eliminating hysteresis

The previous sections have discussed the many factors of hysteresis, and analyzed how various origins cause hysteresisin PSCs. But the dominant factors and main origins can vary with device types. No matter which origin plays a major role in the hysteresis, the hysteresis can be reduced or eliminated by corresponding methods. At present, many methods have been proposed to solve the hysteresisbehavior, including interface engineering, balanced carrier transport, and optimization of the composition and structure of the perovskite. Listed below are some ways to solve the hysteresisissue.

5.1 Optimizing the Perovskite Layer

5.1.1 Composite Engineering

As mentioned earlier, the ion migration characteristics of perovskite materials make ions move in the crystal structure, which leads to structural instability. Therefore, the composition of the perovskite can be optimized by doping to achieve structural stability.

Single-cation or double-cation doping at A site not only can improve the performance of PSCs, but also effectively suppress the hysteresis. By doping the guanidinium cation(Gu^+) into the mixed-cationperovskite ($FA_{0.83}Cs_{0.17}PbI_3$) to replace the FA ions in the lattice, the charge recombination at the interface is reduced and the device with almost no hysteresis is obtained.[113]Recently, a novel quadruple-cation (K, Cs, FA, MA) perovskite has significantly reduced the hysteresis.[114] Attributable to the doping of K ions promotes the crystallization of the perovskite film, increases the charge conductivity and reduces the defect density. Co-doping Cs and Rb into FAMA-based PSCs can also reduce thehysteresis.[115]In addition, the $Cs_{0.2}FA_{0.8}PbI_{2.84}Br_{0.16}$-based PSCs obtained by doping $FAPbI_3$ at the A and X sites also showed negligible hysteresis.[116]

The doping of the B site can not only reduce the toxicity of perovskite, but also obtain PSCs with low hysteresis. Studies have found that Sn-based PSCs show lower hysteresis, and the introduction of Sn at the B site may effectively suppress the hysteresis.[117] For example, $FA_{0.7}Cs_{0.3}Pb_{0.7}Sn_{0.3}I_3$ and $FA_{0.7}MA_{0.3}Sn_{0.3}Pb_{0.7}I_3$ PSCs obtained by introducing Sn elements at B site showed negligible hysteresis.[118,119]Furthermore, applying copper cations (Cu^{2+}) and Cl^- to simultaneously doped B and X sites (co-doping) of $MAPbI_3$ improves the symmetry of the crystal structure.[120] The obtained $MAPb_{0.9}Cu_{0.1}I_{3-2x}Cl_{2x}$-based PSCs can well suppress the hysteresis. Although the PCE of the device is lower than that of $MAPbI_3$-based PSCs, it is very promising in terms of reducing the toxicity of perovskite materials and inhibiting the hysteresis. This provides new insights for

solving the hysteresis behavior. In summary, doping of A, B and X sites can effectively reduce the hysteresis, which is a more commonly used method.

5.1.2 Additive Engineering

Without destroying the composition of the perovskite materials, the morphology of the perovskite film can be optimized through additive engineering to reduce the hysteresis. Additives can be introduced during the preparation of the perovskite film.[121,122] In recent years, ionic liquids have been gradually used in PSCs. Ionic liquid methylammonium acetate (MAAc) as an additive used in two-dimensional (2D) perovskite, which improved the performance and achieved hysteresis-free by affecting the crystallization and morphology of the perovskite film.[123] The moisture-assisted process has also received a lot of attention in recent years.[124] Generally speaking, PSCs are sensitive to water. But an appropriate amount of H_2O helps to prepare smooth and dense high-quality perovskite films and reduce the level of hysteresis.[125] In addition, thiocyanide is also a commonly used additive to suppress the hysteresis. The addition of lead thiocyanate ($Pb(SCN)_2$) in the preparation of perovskite films can significantly increase the grain size, and interact with I ions to form PbI_2 at the GBs to passivate the GBs and alleviate the hysteresis in PSCs.[45] Similarly, the use of KSCN additives can also promote perovskite crystallization to obtain high-quality films, reduce defect density and show lower hysteresis.[126] As shown in the **Figure 8a**, the crosslinkable thioctic acid (TA) can in situ crosslinked to form a polymer (Poly(TA)) network after thermal treatment, effectively passivate defects in the perovskite film.[122] Moreover, the -COOH group in TA can interact

with PbI_2 and TA is chemically bonded to GBs. Therefore, the finally prepared PSCs show negligible hysteresis benefit from the low defect density in the perovskite film.

Currently, fullerenes and their derivatives have been widely used in PSCs. For example, $PC_{61}BM$ and C_{60} can be used as an ETL, and can also be used as additives to reduce the hysteresis. By introducing $PC_{61}BM$ into the perovskite precursor solution to fill the GBs of $MAPbI_3$perovskite, the extraction of carriers is promoted and the hysteresis is significantly reduced while the performance is improved.[127] Further research found that the indene-C_{60} biadduct (ICBA) additive can also passivate defects and promote carrier transport, achieving a more obvious effect than $PC_{61}BM$.[128]Additive engineering is a relatively simple and controllable strategy that optimizes the morphology of the film by controlling the crystallization process, passivates defects and promotes charge transfer to suppress the hysteresis. Although many additives have been found to suppressthe hysteresis, there are still many cost-effective additives waiting for researchers to explore.

5.1.3 Solvent Engineering

The type of solventcan affect the hysteresis for PSCs prepared by the solution process. For example, a systematic study investigated the effect of different solvents on the morphology of MA-based perovskite films and the performance of PSCs, and found that the devices based on mixed solvent DMF/DMSO (dimethylformamide/dimethyl sulfoxide) showed extremely low hysteresis compared to other solvents.[129]In general, the available solvents including DMF, DMSO, gamma-butyrolactone (GBL), methyl-2-pyrrolidone (NMP), MAAc and some mixed

solvents, etc.[129]The molecular structures of some solvents are shown in **Figure 8b**, among which DMF and DMSO are the two most commonly used solvents. Moreover, the preparation process of perovskite film using solution process is generally shown in **Figure 8c**.[130]

The solubility of the perovskite precursor material and the solvent evaporation rate vary with the type of solvent.For example, the films prepared using DMF and GBL have lower density and the device showsinferiorphotovoltaic performance compared to DMSO.[129]This may be due to the different solubility of DMF and GBL to the perovskite precursor material, which leads to poor crystallinity, relatively fast evaporation rate and poor intermediate phase structure stability.Therefore, choosing the right solvent is essential for obtaining high-quality films and low-hysteresis devices. When used high-viscosity and non-toxic MAAc as solvent, a smooth and dense excellent perovskite film can be prepared at room temperature, thereby obtained high-efficiency PSCs without hysteresis.[131]Furthermore, mixed-solvents have greater advantages compared to single solvent.For example, the $MAPbI_3$ film prepared with GBL/DMSO as solvent slows down the crystallization rate, improves the light absorption capacity and effectively inhibits charge recombination, the PSCs showed negligible hysteresis.[132]

5.1.4 2D or 2D/3D Perovskites

In recent years, 2D (or quasi-2D) PSCs have received widespread attention due to their high stability.[133,134] 2D PSCs are divided into three types: Ruddlesden-Popper (R-P) phase, Dion-Jacobson (D-J) phase, and alternate cations in

the interlayer space (ACI).[135,136]If the perovskite can grow perpendicular to the substrate orientation for 2D PSCs, it is conducive to carrier transport.[137] Meanwhile, there is a strong intermolecular force (van der Waals force) between the inorganic layer in the 2D perovskite and the large-sized organic cations, which can effectively inhibit ion migration and thereby alleviate the hysteresis.

There are monovalent organic spacer cations in the 2D R-P phase perovskite, such as n-butylammonium (BA^+, $C_4H_9NH_3^+$), phenylethylammonium (PEA^+, $C_6H_5(CH_2)_2NH_3^+$) or 2-thiophenemethylammonium ($ThMA^+$), etc.[138] Hot-casting or additives induce crystal growth perpendicular to the substrate orientation, so that there are channels for rapid carrier transport in the 2D perovskite, which inhibits charge recombination and significantly reduces level of hysteresis.[139]For example, the 2D R-P phase $(BA)_2(MA)_2Pb_3I_{10}$-based PSCs prepared by the hot-casting method achieved a high PCE of 12.52% without hysteresis.[137] In addition, $(ThMA)_2MA_2Pb_3I_{10}$-based PSCs prepared with MACl as an additive also significantly reduced level of the hysteresis.[139]Meanwhile, control the distribution of 2D perovskite nanoplates with different n values is also important to suppress the hysteresis and improve the photovoltaic performance of PSCs. Hu et al. obtained uniformly arranging different *n* value nanoplates by vacuum poling treatment, which facilitate the directional transfer of carriers.[140] The vertical arrangement of small to large n values is conducive to the balance of carrier transport, which results in excellent performance and lower hysteresis. Similarly, the vacuum-assisted method allows 2D perovskite to be evenly distributed in the film, which helps to charge

transfer and reduces the recombination.[141] Thus, this greatly reduces the hysteresis level.The difference from the R-P phase is that the spacercations used in the D-J phase are divalent organic cations. For example, a novel lead-free 2D (BEA)$FA_2Sn_3I_{10}$ (BEA=1,4-butanediamine) PSCs shows negligible hysteresis.[142] The introduction of BEA cation can not only stabilize the perovskite structure, but also inhibit the oxidation of Sn^{2+}.Meanwhile, ACI-phase perovskite can also effectively suppress the hysteresis. 2D B-ACI type $(BEA)_{0.5}MA_3Pb_3I_{10}$-based PSCs showed efficiency of 14.86% and negligible hysteresis.[143] This is due to the fact that this 2D perovskite provides a carrier positioning process, which enhances carrier mobility and balances carrier transport.

Although 2D PSCs have higher stability and lower hysteresis, they have lower PCE than three-dimensional (3D) PSCs. Combining the advantages of 2D and 3D perovskites, it is a feasible method to prepare high-efficiency, stable and low hysteresis 2D/3D hybrid perovskites.[144]The 2D-3D heterostructured $BA_{0.09}(FA_{0.83}Cs_{0.17})_{0.91}Pb(I_{0.6}Br_{0.4})_3$ PSCs obtained by introducing a small amount of BA cation into the 3D perovskite has lower hysteresis compared with 3D $FA_{0.83}Cs_{0.17}Pb(I_{0.6}Br_{0.4})_3$.[145]The introduction of BA obtained plate-like 2D perovskite crystallites perpendicular to the substrate and inserted into the 3D perovskite, the charge recombination is greatly reduced (**Figure 8d**). Furthermore, the Sn-based 2D/3D perovskite with low defect density prepared by introducing PEA cation with SnF_2 as the reducing agent effectively promotes charge collection, and exhibits negligible hysteresis at different scan rates.[146]This benefits from the 2D perovskite at

the bottom can induce the orientation growth of 3D perovskite crystals to obtain the film with good crystallinity.

5.1.5 Select the Appropriate Preparation Method

Uniform, smooth and high coverage high-quality perovskite films are necessary to obtain high-performance PSCs. A satisfactory film morphology can be obtained by select an appropriate preparation method, which helpstosuppress the hysteresis. At present, the most commonly used method is the solution process, including one-step and two-step methods.[147]The one-step method can synthesize perovskite films more quickly, but requires an anti-solvent to assist crystallization. The operation of the two-step method is relatively complicated. First, spin-coating an inorganic precursor to obtain an inorganic film, and then spin-coating an organic precursor solution to obtain the perovskite film. Generally, the perovskite film prepared by the solution process contains numerous GBs, which will hinder carrier transport and affect the performance of device. Therefore, it is necessary to optimize the preparation method to adjust the grain size and film morphology to reduce the hysteresis.

For example, used a poly(ethylene oxide) (PEO) co-crystallized method.[148]Applicationof PEO inhibits the migration of counter ions (I^- and MA^+), and forms hydrogen bonds with perovskites andsuppress the formation of point defects, promotes carrier transport and finally obtains hysteresis-free device.In order to prepare high-quality films under environmental conditions, preformed perovskite powder can be used to prepare perovskite precursor solutions.[149] As shown in the **Figure9a**, the perovskite powder is prepared by anti-solvent recrystallization method.

And the prepared perovskite film has good crystallinity and excellent morphology, which significantly alleviates the hysteresis.[149]Vapor deposition technology is also a common preparation method in recent years. For example, the large area $FA_{0.81}MA_{0.15}PbI_{2.51}Br_{0.45}$-basedPSCsprepared by the vacuum flash-assisted solution process (VASP) has a smooth, uniform perovskite film with fewer GBs, thereby the final device shows negligible hysteresis.[150]The process of preparing perovskite film via VASP is shown in **Figure 9b**. In addition, a novel three-step preparation process has also been proposed, resulting in devices with negligible hysteresis.[151]

In addition to exploring new preparation techniques, the annealing temperature and substrate temperature can also be adjusted to alleviate the hysteresis. The annealing temperature can affect the crystallization process of the perovskite films, the grain size and surface morphology. For example, the perovskite film prepared by the two-step annealing technique (indirect contact annealing followed by direct contact annealing) shows different levels of hysteresis at different annealing temperatures.[152]Under certain conditions, the gradient thermal annealing process (rise from low temperature to high temperature at a certain heating rate, and continue annealing at high temperature for a certain period of time) has better surface morphology and lower hysteresis than direct annealing.[153]In addition, hot-casting method has also been used, the preparation process is shown in **Figure 9c**.[154] The film prepared by the hot-casting method has larger grain size after post-annealing, reducethe defects of GBs and eliminates the influence of environmental humidity, thereby the obtained PSCs shows low hysteresis.[154,155] In short, the preparation

method can affect the quality of the film, and an appropriate method should be selected to prepare PSCs.

5.1.6 Heterojunction Engineering

PSCs with planar heterojunction (PHJ) structure often suffer from the hysteresis, which can be effectively suppressed by heterojunction engineering. For PSCs, there are three common heterojunction structures: PHJ, bulk heterojunction (BHJ), and gradient heterojunction (GHJ).[156]Relative to the normal PHJ structure with the electron acceptor as the intermediate layer. In the BHJ structure, the electron acceptor are evenly dispersed in the perovskite layer. The electron acceptorare distributed in gradienton the interface of the perovskite layer/ETL in the GHJ structure. As shown in the **Figure9d**, it is schematic diagram of three types of heterojunction structures.[156]

Generally, fullerenes and their derivatives are widely used to form BHJ due to their good conductivity. The resultedBHJ has highcarrier mobility and low trap state density, which promotes carrier extraction and effectively suppress the hysteresis.[157,158] For example, pyridine-functionalized fullerene derivative (C_{60}-PyP) can provide heterogeneous nucleation sites and increase the grain size.[159] In addition, the coordination between some of the nitrogen (N) atoms in pyridine and Pb^{2+} ions can passivate the trap state, so that the BHJ PSCs prepared by adding C_{60}-PyP exhibits negligible hysteresis. Except for the commonly used fullerene derivatives, small molecules and inorganic materials can also be added to form BHJ. A small molecule material

3,9-bis(2-methylene-(3-(1,1-dicyanomethylene)-indanone))-5,5,11,11-tetrakis(4-hexyl phenyl)-dithieno[2,3-d:2′,3′-d′]-s-indaceno[1,2-b:5,6-b′] dithiophene (ITIC)can enhance the light absorption capacity and improve the electron mobility, which largely suppresses the hysteresis.[160] Inverted BHJ PSCs (ITO/PTAA/BHJ $MAPbI_{2.55}Br_{0.45}$-Zn_2SnO_4/$PC_{61}BM$/Al) shows lower hysteresis than PHJ, due to the addition of Zn_2SnO_4 which makes the film have a good morphology, inhibits charge recombination and balance the carrier transport.[161]On the other hand, the GHJ structure facilitates collection of carrier and inhibits charge recombination, thereby show higher PCE and lower hysteresis.[156]**Figure 9e** shows the preparation methods of three PSCs with heterojunction structure.[162]

5.2 Improving Performance of ETL

As mentioned in **Section 3.2.1**, the material, morphology, and structure of the ETL has significant impact on the hysteresis. Therefore, choosing appropriate materials and structures to improve the performance of the ETL can effectively suppress the hysteresis. In this section, some methods to reduce or eliminate the hysteresis are listed from the ETL level.

5.2.1 Improve TiO_2 ETL Performance to Reduce Hysteresis

At present, TiO_2 is the most commonly used ETM.[163,164] However, the conductivity of TiO_2 (0.00006 $mS \cdot cm^{-1}$) is relatively low and the defect density of TiO_2 film is relatively high. This is not be conducive to the rapid extraction of carriers and lead to charge recombination, eventually make PSCs show hysteresis. Doping

other materials or optimizing the TiO_2 nanostructure can obtain high-quality TiO_2 ETL and reduce the hysteresis.

For doping, Li,[165] Ta,[166] Nb,[167] Pt,[168] Ru,[169] Co[170] and Al[171] have been doped into the mp-TiO_2 or c-TiO_2 layer, showed a lower hysteresis than pure TiO_2-based PSCs. For Pt-doped c-TiO_2 as ETL, the doping of Pt changes the energy level of TiO_2 and enhances the electron mobility and charge extraction ability of TiO_2, thus show lower hysteresis (**Figure 10a,b**).[168]After Li is doped into mp-TiO_2, it passivates the defects in the ETL, reduces the number of charge recombination centers and accelerates the electron transport speed, so that the prepared device exhibits negligible hysteresis.[165]Likewise, doping Ru into mp-TiO_2 results in a high-quality TiO_2 film, which also promotes charge transport and collection, and effectively reduces the hysteresis.[172] The performance of PSC obtained by TiO_2 ETL with various elements doping are listed in **Table 2**.

For ETL prepared from mp-TiO_2 nanoparticles, the photovoltaic performance of the device is limited due to its low electron mobility. Improving the nanostructure of mp-TiO_2 can not only increase PCE of device, but also effectively reduce the level of hysteresis. As an example, the 670 nm length of mp-TiO_2 nanorods as ETL significantly suppress the hysteresis.[173] This can be attributed to the fact that the mp-TiO_2 nanorods reduce the defect density and charge accumulation at the contact interface with the perovskite layer, which greatly promotes charge extraction. The carrier extraction and accumulation process of the planar TiO_2 and nanorods as shown in **Figure 10c**. In addition, the nanotube and nanowire structured TiO_2 as ETL can

enhances the light absorption capacity and promotes carrier transport, and the fabricated device also shows low hysteresis.[174]

5.2.2 Other ETM with Excellent Performance

In recent years, researchers have been exploring the application of ETM with excellent performance to planar PSCs to suppressthe hysteresis. SnO_2 has a higher electron mobility and lower conduction band energy level compared with TiO_2. Therefore, it has received extensive attention as an ETL.[175] Under low temperature conditions, SnO_2 prepared by atomic layer deposition (ALD) technology has better energy level matching with the perovskite layer, which is beneficial to the separation and collection of carriers, and exhibits low hysteresis at different scan rates.[53]Using ZnO as the ETM has also achieved outstanding results for reduce the level of hysteresis. It has a similar energy level to that of TiO_2, but its conductivity (0.0031 $mS \cdot cm^{-1}$) is higher than that of TiO_2 and the preparation process is simpler.[176] In addition, some other inorganic transport materials, such as α-Fe_2O_3,[177] Zn_2SnO_4,[178] ZnSe,[179] $SrTiO_3$ (Nb doped and treated with HCl)[180] can also be used as ETL to suppressthe hysteresis.

In addition to inorganic semiconductor materials, organic materials such as fullerenes and their derivatives can also be used as ETL for planar PSCs. For instance, C_{60} and $PC_{61}BM$ as ETL have been widely used in planar PSCs.[181] The $PC_{61}BM$ ETL with rough surface prepared by spraying technology can form a cross-linked network and promote charge extraction, obtained an PCE of more than 17% and showed lower hysteresis.[182]The PSCswithFTO/C_{60}/$MAPbI_3$/carbon structure

achieved a high efficiency of 15.38% without hysteresis, due to the fact that C_{60} can promote charge extraction and reduce the sub-band gap state at the interface.[183] Other organic materials such as [6,6]-phenyl C_{71} butyric acid methyl ester ($PC_{71}BM$),[184] fulleropyrrolidinium iodide (C_{60}-bis),[185] poly(9,9-dioctyfluorene-co-benzothiazole) (F8BT),[186] N,N¢′-bis(3-(dimethylamino)propyl)-5,11-dioctylcoronene-2,3,8,9-tetracar-boxdiimide (CDIN),[187] indacenodithieno[3,2-b]thiophene (IT) like (IT-like)[188] can also effectively suppress or eliminate the hysteresis. Moreover, the solid ionic liquid (ss-IL) with high conductivity and electron mobility as ETL can significantly reduce the defect density and effectively suppress the hysteresis.[189]

Doping with other elements or special treatment can further improve the performance of the above-mentioned ETL. As an example, gallium-doped SnO_2(Ga-SnO_2) ETL not only has a more excellent energy level, but also Ga doping reduces the trap state density in the ETL, thus promotes the extraction and transfer of electron.[190] Consequently, the devices prepared by either the one-step or the two-step method show higher efficiency and lower hysteresis.In another study, BHJ ETL composed of $PC_{61}BM$ and poly[N-9′-heptadecanyl-2,7-carbazole-alt-5,5-(4′,7′-di-2-thienyl-2′,1′,3′-benzothiadiazole)] (PCDTBT) was used in PSCs with inverted structure.[32] The electron mobility is greatly improved and the charge trapping area is reduced compared with $PC_{61}BM$. Compared with $PC_{61}BM$-based PSCs, the efficiency is increased by about 15% and the hysteresis is negligible.Furthermore, yttrium (Y)-doped SnO_2nanosheets,[191]

graphitic carbon nitride (g-C_3N_4)-doped SnO_2,[192]poly[9,9-bis(6′-(N,N-diethylamino)propyl)-fluorene-alt-9,9-bis(3-ethyl (oxetane-3-ethyloxy)-hexyl) fluorene] (PFNOX)-doped $PC_{61}BM$,[193]indium (In)-doped ZnO nanofibers[194] and N-doped ZnO nanosheets[195] also have important reference significance in reduce hysteresis and improve performance of PSCs.In addition to doping with other elements, the application of new preparation techniques can also improve performance and suppress the hysteresis. The internal porous ZnO material prepared by the Metal-Organic-Framework (MOF)-derived technology is used as the ETL.[196] Comparedwith the traditional ZnO nanoparticles, the light harvesting ability is improved, the charge extraction is promoted and the recombination probability is reduced.The formation process of MOF-derived ZnO and the process of enhance light harvesting and charge separation as ETL are shown in the **Figure 10d**. Finally, the device with 18.1% efficiency and no hysteresis was obtained.

5.2.3 Bi-ETL and ETL-Free

The ETL with bi-layer structure (bi-ETL) has been extensively studied due to its excellent electron transport and stability.[197] Using bi-ETL in PSCs can not only improve PCE but also reduce the level of hysteresis, such as $PC_{61}BM/C_{60}$,[54] $PC_{61}BM$/AZO (Al-doped ZnO),[198] barium hydroxide/boron-doped ZnO,[199] $Nb_2O_5/PC_{61}BM$,[200] C_{60}/ultrathin-TiO_x,[201] and bi-layer SnO_2[23].The bi-layer SnO_2 (a layer of colloidal SnO_2 spin-coated on the sol-gel SnO_2) as the ETL has better energy level alignment with the perovskite and accelerates the charge extraction.[23]It has lower hysteresis compared with single SnO_2 ETL.When single $PC_{61}BM$ is used as an

ETL, heat treatment is required to achieve the effect of suppress the hysteresis; when the $PC_{61}BM/C_{60}$ bi-ETL is used, C_{60} can effectively passivate the defects of GBs to promote charge transfer without heat treatment, and hysteresis-free PSCs is obtained.[54] The charge transfer processes of $PC_{61}BM$ ETL and $PC_{61}BM$ /C_{60} bi-ETL are shown in **Figure 10e**.

In order to deal with some problems encountered when TiO_2 is used as ETL, some researchers have begun to explore the structure of PSCs without ETL. Used tetramethylammonium hydroxide (TMAH) to modify the surface of FTO to prepare PSCs without ETL.[202] The highest PCE reached 20.1% and the hysteresis was effectively reduced. This result can be attributed to the fact that TMAH can not only improve the surface and electrical properties of FTO by forming a surface dipole layer, but free TMA^+ can also enter the perovskite layer to reduce trap density and enhance the conductivity of perovskite layer. Recently, used an additive-assisted strategy to prepare a novel ETL-free bilayer (the bottom is dense layer and the top is maze-like layer)perovskite film PSCs that achieved high PCE of 18.5% and showed negligible hysteresis.[203] As shown in the **Figure 10f**, the high PCE and low hysteresis can be ascribed to the maze-like perovskite film which increases the interface contact and promotes separation and transfer of hole.

5.3 Improving Performance of HTL

Except for PSCs with inverted p-i-n structure, Spiro-OMeTAD is the most widely used HTM in PSCs. However, the hole mobility (~ 10^{-4} $cm^2 \cdot V^{-1} \cdot s^{-1}$) and conductivity (0.01 $mS \cdot cm^{-1}$) of Spiro-OMeTAD are low, which is not conducive to

carrier transport.[204] This will affect the performance of PSCs and cause the *J-V*hysteresis. Therefore, it is necessary to dope other materials to adjust the performance of Spiro-OMeTAD HTL or select excellentHTM to effectively solve these problems.

5.3.1 Optimize Spiro-OMeTAD HTL

In order to improve the performance of Spiro-OMeTAD HTL, it is generally doped with Li-TFSI, tBP or tris[2-(1H-pyrazol-1-yl)-4-tert-butylpyridine]cobalt-(III)tris[bis(trifluoromethylsulfonyl)imide] (FK209).[205] Li^+ in Li-TFSI can oxidize Spiro-OMeTADand $TFSI^-$ can stabilize Spiro-OMeTAD.[206] However, the hydrophilic nature of Li-TFSI can cause the HTL to deliquesce by absorbing water, and Li^+can migrate into the perovskite layer to increase the defect density of the HTL.[207]The tBP as polar substance can enhance the polarity of HTL to achieve good interface contact, but tBP can react with perovskite to degrade the perovskite light-absorbing layer.[208]In addition, acetonitrile (ACN, a polar solvent commonly used to dissolve Li-TFSI and FK209)will corrode perovskites. Although the doping of these materials can improve the efficiency of the device, the instability of thesematerials will hinder its further development. Therefore, it is urgent to find more suitable dopants or other modification methods to optimize Spiro-OMeTAD HTL.

In addition to the above three dopants, non-hygroscopic 2,3,5,6-tetrafluoro-7,7,8,8-tetracyanoquinodimethane (F4-TCNQ) has also begun to be gradually applied to the doping of Spiro-OMeTAD.[209] F4-TCNQ instead of

Li-TFSI + tBP as dopant can effectively reduce series resistance and promote hole transport, and F4-TCNQ can passivate the trap states on the surface of the perovskite layer, thereby showing lower hysteresis (**Figure 11a-c**). Moreover, F4-TCNQ improves the hydrophobicity of HTL compared with the typical Li-TFSI + tBP dopant, thus shows better stability.Liao et al. used MoS_2 with a flower-like microstructure to modify Spiro-OMeTAD doped with Li-TFSI and tBP.[207] MoS_2 can adsorb Li^+ to inhibit its migration, and increase the hole mobility of Spiro-OMeTAD (**Figure 11d**).The corresponding devices show higher efficiency and lower hysteresis.In order to solve the problem of ACN solvent, a more suitable solvent can be selected to replace ACN. Using isopropanol (IPA) as the solvent of Li-TFSI greatly reduces the corrosion of the perovskite film, reduces the charge recombination and finally improves efficiency of the device and significantly suppresses the hysteresis.[210]Recently, the fluorinated isomeric analogs (Spiro-mF) of Spiro-OMeTAD as an HTL can also reduce the hysteresis.[211] Spiro-mF not only has better energy levels, but also can effectively suppress non-radiative recombination. Finally, Spiro-mF-based PSCs not only obtains better photovoltaic performance, but also shows superior stability compared with Spiro-OMeTAD.

5.3.2 Select the Appropriate Materials and Doping

In addition to Spiro-OMeTAD, other organic materials such as PTAA,[212,213] PEDOT:PSS,[62,214] and poly(3-hexylthiophene) (P3HT)[215] have also been used as HTM in PSCs. Moreover, the poly[2-methoxy-5-(2-ethylhexyloxy)-1,4-phenylenevinylene] (MEH-PPV) as an

HTM has a better HOMO energy level, and hysteresis-free device is prepared.[216] The x-shaped organic material 4,4′,4″,4‴-silanetetrayltetrakis(N,N-bis(4-methoxyphenyl)aniline) (Si-OMeTPA) has higher hole mobility and good thermal stability, and it shows lower hysteresis as HTL in PSCs.[217]Although these organic materials can effectively suppress the hysteresis, stabilityandprice issues have always hindered their practical application.

Many relatively inexpensive inorganic materials have also been developed as HTL for PSCs, which have higher stability than organic materials.[218] Among them, NiO_x is an excellent inorganic HTM commonly used in inverted structure devices. NiO_x as an HTL can effectively suppressthe hysteresis, and can be further modified to improve performance.[219] Recently, $NiCo_2O_4$ has also shown good performance as HTL, and the hysteresis is obviously suppressed.[220] Some inorganic materials containing copper have also been used as HTL, such as CuSCN,[221] CuI,[221]CuS,[56]Cu_2ZnSnS_4,[222]copper phthalocyanine (CuPc)[223] and CuO_x[224]. For example, CuSCN as HTL has a high hole mobility and suitable energy level, which can promote carrier transport at the interface.[225] Thus, devices based on CuSCN have lower hysteresis.Although these inorganic materials have high stability and can effectively suppress the hysteresis, but the efficiency of device is relatively low. Therefore, other materials need to be explored to improve efficiency.

The above alternative materials can effectively suppress hysteresis, and adding dopants can further improve the performance of these HTLs to increase efficiency and suppress the hysteresis. For example, a fluorine-containing Lewis acid dopant (LAD)

and PTAA can form an adduct PTAA-LAD, which increases the hole mobility and reduces the HOMO energy level.[226]In addition, LAD can form supramolecular interaction with halide ions through halogen bonds, resulting in passivation of trap states(**Figure 11e**).Compared with Li-TFSI + tBP-doped PTAA-based PSCs, it shows higher efficiency, lower hysteresis and better stability. Doping F8BT into PTAA can also significantly suppress the hysteresis.[227] In addition, Cu-doped NiO_x as HTL has also been proven to improve efficiency of device without hysteresis, and shows good stability.[228]

5.4 Interface Engineering

The interface playsimportant role in the hysteresis. For example, a large number of defects at the interface can cause charge recombination and hinder the extraction and transport of carriers. Taking the typical PSCs with planar n-i-p structure as an example, the interface between each functional layer may affect the hysteresis. Interface engineering has always been considered an effective method to enhance the performance of PSCs and suppress the hysteresis. Interface engineering can improve interface performance, effectively promote carrier separation and extraction, thereby suppress or eliminatethe hysteresis.

5.4.1 Interface Modification

Interface modification can adjust the band arrangement, promote carrier transport, enhance performance of device and suppress the hysteresis. For example, using 5-amino-2,4,6-triiodoisophthalic acid (ATPA) to optimize the TiO_2 ETL/inorganic

$CsPbI_3$ perovskite layer interface, a high efficiency of 18.2% was obtained and the hysteresis was significantly suppressed.[229] This is because ATPA optimizes the energy level arrangement between TiO_2 and perovskite to promote charge extraction, and ATPA can passivate defects on the surface of the perovskite film to reduce interface recombination (**Figure 12a**). The ionic liquid 1-butyl-3-methylimidazolium tetrafluoroborate ($BMIMBF_4$) modified the ETL/perovskite interface can also reduce the hysteresis.[230] $BMIMBF_4$ can not only modify the surface of n-type oxide ETL, but also adjust the Fermi level (closer to the conduction band) to promote electron transport.Recently, an organophosphorus ligand triphenylphosphine oxide (TPPO)was developed to achieve interface modification.[231] TPPO can passivate defects by forming Pb-O bond with uncoordinated Pb^{2+}, and the benzene ring contained in it can promote charge transfer at the interface, so that the modified device shows lower hysteresis.The interface modification of other materials such as fullerene and its derivatives can also improve device performance and suppress the hysteresis.[232]

For the HTL/perovskite layer interface, the introduction of 3-aminopropanoic acid self-assembled monolayer (C3-SAM) between the PEDOT:PSS and the perovskite layer improves the crystalline quality and surface morphology of the perovskite film, which can effectively alleviatethe hysteresis and does not depend on the scan rate.[233] The application of 4-tert-butyl-benzylammonium iodide (tBBAI) can optimize the interface performance between perovskite/Spiro-OMeTAD, improve PCE of device and reduce hysteresis.[234] This is mainly because tBBAI can passivate the interface defects between perovskite/Spiro-OMeTAD and promote the extraction

and transport of carriers (**Figure 12b**).Moreover, modifying the interface between FTO/ETL can also alleviate hysteresis. For example, using $SnCl_4$ to optimize the interface between the FTO substrate and SnO_2 can enhance electronic coupling and achieve interface passivation, thereby the hysteresis is effectively reduced.[235]The above examples all indicate the importance of interface modification to suppress the hysteresis.

5.4.2 Insert the Interlayer

The introduction of an interlayer between two functional layers can also effectively suppress the hysteresis. The introduction of the interlayer can not only passivate defects to reduce the charge recombination, but also more effectively block the opposite carriers from entering the carrier transport layer. And the introduction of the interlayer will not affect the overall light transmittance of the device. Recently, In_2O_3 as an interlayer between the TiO_2 ETL and the perovskite layer has significantly suppressed hysteresis and improved PCE of device.[236]The In_2O_3 interlayer can result in a smoother perovskite film, which reduces the charge recombination sites at the interface and enhances the electron transport performance. Inserting a thin layer of MgO and ethanolamine (EA) between the ZnO ETL and the perovskite layer can obtain an efficient and hysteresis-free device(**Figure 12c**).[237] This can be attributed to MgO can reduce interfacial charge recombination, and EA can promote carrier transport. The use of fullerene derivatives in interface engineering can also alleviate the hysteresis, due to their ability to passivate the surface defects of ETL and improve the electron transport performance.[238]

Similarly, inserting an interlayer between the perovskite layer and the HTL can also alleviate the hysteresis. Mesoporous Al_2O_3 has been reported to be used as an interlayer in inverted PSCs to suppress the hysteresis.[239] As shown in the **Figure 12d**, Al_2O_3 can not only block electrons but also effectively block the shunt pathways between HTL/ETL.In addition, natriumion-functionalized carbon nano-dots(CND@Na) can be used as interlayer materials to modify the PTAA/perovskite layer interface.[240]CND@Na not only helps to passivate surface defects and inhibit interface recombination, but also controls the order and crystal size of perovskite, thereby obtain efficient and stable PSCs and significantly suppressthe hysteresis (**Figure 12e,f**).Recently, 2D interlayer has also been proposed to effectively reduce the level of hysteresis. The introduction of 2D perovskite layer at the perovskite/HTL interface can inhibit ion diffusion at the interface or improve charge extraction, thereby reducing the level of hysteresis.[241] The use of a 2D n-BAI layer for double-sided passivation of the 3D perovskite film can effectively passivate the defects at the interface and inhibit the recombination of carriers, which improves cell efficiency and reduces the hysteresis.[242]

In addition to the ETL/perovskite/HTL interface, inserting an interlayer between the carrier transport layer and the electrode also has a greater effect on suppress hysteresis. Bathocuproine (BCP) is often used in PSCs with p-i-n structure, and its hole blocking ability helps to alleviate the hysteresis. Inserting a proper thickness of BCP between the PCBM and the Ag electrode can form an ohmic contact and reduce interface recombination and interface charge accumulation, which can improve the

efficiency of PSCs and alleviate the hysteresis.[243]

6. Conclusion and Outlook

Although the current research on the mechanism of hysteresis and the strategies to suppress hysteresis have greatly promoted our understanding of hysteresis, there are still some problems that need further research to promote the development of PSCs.Based on this, we believe that the following aspects have great significance in promoting hysteresis research and the development of PSCs：

- **Discover the origin of hysteresis in PSCs**

The origin of hysteresis has always been the focus of debate in hysteresis research. Although current research has proposed some possible origins of hysteresis, these origins have been questioned and challenged.At the same time, some studies believe that the hysteresis may be caused by multiple possible origins, but the relationship between these origins has not been systematically clarified.Moreover, many strategies to suppress the hysteresis are carried out only for one of the possible origins. Although these strategies can effectively suppress the hysteresis, there is still a long way to achieve hysteresis-free.Determining the origin of hysteresis is conducive to targeted resolution of hysteresis,but finding the exact origin of the hysteresis still requires a lot of effort. Therefore, systematic research to determine the origin of the hysteresis or clarify the relationship between the current possible origins is essential to solve the hysteresis in the future.

- **Develop more comprehensive HTMto suppress the hysteresis**

Choosing the appropriate HTM helps to suppress the hysteresis, and the development of excellent HTM has become a hot spot on PSCs research. At present, the HTM used in most studies is organic materials (such as Spiro-OMeTAD and PTAA), but its stability and price issues have always hindered the further development in hysteresis. In recent years, due to the outstanding advantages of inorganic HTM such as good stability and low price, more and more researchers have begun pay attention to the application of inorganic HTM in hysteresis.However, the PCE of devices prepared with inorganic HTM is generally lower than that of organic HTM. It is what we expect to reduce the level of hysteresis without losing the performance of the PSCs. Therefore, develop theefficient HTMs with superior properties (such as high stability, low price, high hole mobility and excellent energy level for hole extraction) in the future will not only help to solve the hysteresis issue, but also achieve a balance between cost and performance.

- **Research on the mixed hysteresis**

As mentioned earlier, it is called mixed hysteresis when the RS and FS curve intersect at a point. We can simply think that normal hysteresis and inverted hysteresis coexist in this case. However, current research mainly focuses on the normal hysteresis or inverted hysteresis, and there is a lack of systematic research on mixed hysteresis. We don't know what mechanism may cause the mixed hysteresis, which make it particularly difficult to solve this type of hysteresis. Therefore, systematic research on the mixed hysteresis in the future to determine its generation mechanism will help to strengthen our understanding of this phenomenon, and also help us choose better

methods to solve the hysteresis issue. We believe that the research on mixed hysteresis can accelerate the process of discover the origin of hysteresis, and promote the early practical application of PSCs.

- **The connection between stability of device and hysteresis**

The severe hysteresis can cause instability of PSCs.[244]Some origins of hysteresis can also greatly affect the stability of the device.For example, ion migration leads to unbalanced element distribution in the perovskite film and unstable crystal structure, which in turn leads to poor long-term stability of the device.Therefore, the relationship between hysteresis and stability needs to be clarified.In future research, it is important to study how hysteresis causes instability of device and to establish a clear relationship between them. In addition, we can also observe whether the suppression effect on hysteresis is effective against a long time after using different strategies to suppress the hysteresis.And whether the application of this strategy will reduce the stability of the device should also be considered.This can illustrate the long-term suppression effect of this strategy.Based on our understanding, it is possible to study the hysteresis changes of the device after long-term operation under extreme environments (high temperature, high humidity, ultraviolet radiation).

- **Whether the application of bi-ETL structure will lead to new interface trouble**

The interface is one of the main areas of charge recombination and charge accumulation. The nature of the interface can affect the photovoltaic performance and hysteresis of PSCs, which has always been the focus of researchers. As described in

Section 5.2.3, PSCs with bi-ETL structure have a relatively low hysteresis. However, the introduction of bi-layer structure will inevitably increase the number of interfaces. What role the newly introduced interface plays in hysteresis needs to be clarified. Furthermore, whether the newly introduced interface will cause more serious interface energy loss and whether it will affect the stability of the device should be considered. Suppression of hysteresis should not be at the expense of efficiency and stability of device. But the current research on this issue is still insufficient. Therefore, more researchers are required to make efforts to provide us with accurate and useful information. This has great reference significance and can also promote the development of PSCs with bi-ETL structureto suppress the hysteresis.

In summary, hysteresis is animportant problem that needs to be solved urgently in research of PSCs. More efficient methods should be developed to suppress or eliminate the hysteresis from different perspectives.The performance and morphology of the perovskite layer can be effectively improvedthrough composite engineering, heterojunction engineering, additive engineering and other methods, thereby effectively reduce the level of hysteresis. The modification of commonly used ETM (HTM) or the development of other excellent ETM (HTM) can promote the balance of carrier transport, and can also suppress or eliminate the hysteresis. For the interface, modify the interface in different ways or introduce an interlayer has great significance for improving the performance of interface and suppressing the hysteresis.Finally, future research can focus on the connection between various possible origins or the discovery of the accurate origin of hysteresis. Meanwhile, studying the mechanism of

mixed hysteresis and the development of more excellent materials for PSCs also help to suppress the hysteresis.

Acknowledgements

This work was funded by the National Natural Science Foundation of China (51902148, 61704099, 61874166, U1832149, 51801088 and51802024), the Fundamental Research Funds for the Central Universities (lzujbky-2020-61, lzujbky-2019-88 and lzujbky-2020-kb06), and the Special Funding for Open and Shared Large-Scale Instruments and Equipments of Lanzhou University (LZU-GXJJ-2019C023 and LZU-GXJJ-2019C019).

Competing Financial Interests

The authors declare no competing financial interests.

References：

[1] S. Bai, P. Da, C. Li, Z. Wang, Z. Yuan, F. Fu, M. Kawecki, X. Liu, N. Sakai, J.T.-W. Wang, S. Huettner, S. Buecheler, M. Fahlman, F. Gao, H.J. Snaith, *Nature* **2019,***571*, 245.

[2] Y. Wang, M.I. Dar, L.K. Ono, T. Zhang, M. Kan, Y. Li, L. Zhang, X. Wang, Y. Yang, X. Gao, Y. Qi, M. Grätzel, Y. Zhao, *Science* **2019,***365*, 591.

[3] Q. Wang, Z. Jin, D. Chen, D. Bai, H. Bian, J. Sun, G. Zhu, G. Wang, S. Liu, *Adv. Energy Mater.* **2018,***8*, 1800007.

[4] D. Barrit, P. Cheng, K. Darabi, M.-C. Tang, D.-M. Smilgies, S. Liu, T.D. Anthopoulos, K. Zhao, A. Amassian, *Adv. Funct. Mater.* **2020,***30*, 1907442.

[5] W. Zhu, W. Ma, Y. Su, Z. Chen, X. Chen, Y. Ma, L. Bai, W. Xiao, T. Liu, H. Zhu, X. Liu, H. Liu, X. Liu, Y. Yang, *Light: Sci. Appl.* **2020,***9*, 112.

[6] A. Kojima, K. Teshima, Y. Shirai, T. Miyasaka, *J. Am. Chem. Soc.* **2009,***131*, 6050.

[7] C. Yan, Z. Li, Y. Sun, J. Zhao, X. Huang, J. Yang, Z. Ci, L. Ding, Z. Jin, *J. Mater. Chem. A* **2020,***8*, 10346.

[8] NREL, *https://www.nrel.gov/pv/assets/pdfs/best-research-cell-efficiencies.20200922.pdf (accessed: September 2020)*.

[9] W. Hu, H. Cong, W. Huang, Y. Huang, L. Chen, A. Pan, C. Xue, *Light: Sci. Appl.* **2019,***8*, 106.

[10] Y. Yang, J. Wu, X. Wang, Q. Guo, X. Liu, W. Sun, Y. Wei, Y. Huang, Z. Lan, M. Huang, J. Lin, H. Chen, Z. Wei, *Adv. Mater.* **2020,***32*, 1904347.

[11] T.-Y. Yang, N.J. Jeon, H.-W. Shin, S.S. Shin, Y.Y. Kim, J. Seo, *Adv. Sci.* **2019,***6*, 1900528.

[12] H.J. Snaith, A. Abate, J.M. Ball, G.E. Eperon, T. Leijtens, N.K. Noel, S.D. Stranks, J.T.-W. Wang, K. Wojciechowski, W. Zhang, *J. Phys. Chem. Lett.* **2014,***5*, 1511.

[13] H.-H. Fang, F. Wang, S. Adjokatse, N. Zhao, J. Even, M. Antonietta Loi, *Light: Sci. Appl.* **2016,***5*, e16056.

[14] Q. Jiang, Y. Zhao, X. Zhang, X. Yang, Y. Chen, Z. Chu, Q. Ye, X. Li, Z. Yin, J. You, *Nat. Photon.* **2019,***13*, 460.

[15] W. Li, M.U. Rothmann, A. Liu, Z. Wang, Y. Zhang, A.R. Pascoe, J. Lu, L. Jiang, Y. Chen, F. Huang, Y. Peng, Q. Bao, J. Etheridge, U. Bach, Y.-B. Cheng, *Adv. Energy Mater.* **2017,***7*, 1700946.

[16] E.M. Sanehira, A.R. Marshall, J.A. Christians, S.P. Harvey, P.N. Ciesielski, L.M. Wheeler, P. Schulz, L.Y. Lin, M.C. Beard, J.M. Luther, *Sci. Adv.* **2017,***3*, eaao4204.

[17] H. Yao, F. Zhou, Z. Li, Z. Ci, L. Ding, Z. Jin, *Adv. Sci.* **2020,***7*, 1903540.

[18] L. Gu, Z. Fan, *Light: Sci. Appl.* **2017,***6*, e17090.

[19] H. Rao, S. Ye, W. Sun, W. Yan, Y. Li, H. Peng, Z. Liu, Z. Bian, Y. Li, C. Huang, *Nano Energy* **2016,***27*, 51.

[20] L. Xiong, M. Qin, C. Chen, J. Wen, G. Yang, Y. Guo, J. Ma, Q. Zhang, P. Qin, S. Li, G. Fang, *Adv. Funct. Mater.* **2018,***28*, 1706276.

[21] G.A. Nemnes, C. Besleaga, A.G. Tomulescu, L.N. Leonat, V. Stancu, M. Florea, A. Manolescu, I. Pintilie, *J. Mater. Chem. C.* **2019,***7*, 5267.

[22] K. Yao, F. Li, Q. He, X. Wang, Y. Jiang, H. Huang, A.K.Y. Jen, *Nano Energy* **2017,***40*, 155.

[23] L. Lin, T.W. Jones, J.T.-W. Wang, A. Cook, N.D. Pham, N.W. Duffy, B. Mihaylov, M. Grigore, K.F. Anderson, B.C. Duck, H. Wang, J. Pu, J. Li, B. Chi, G.J. Wilson, *Small* **2020,***16*, 1901466.

[24] P. Liu, W. Wang, S. Liu, H. Yang, Z. Shao, *Adv. Energy Mater.* **2019,***9*, 1803017.

[25] M. Saliba, T. Matsui, K. Domanski, J.-Y. Seo, A. Ummadisingu, S.M. Zakeeruddin, J.-P. Correa-Baena, W.R. Tress, A. Abate, A. Hagfeldt, M. Grätzel, *Science* **2016,***354*, 206.
[26] P. Umari, E. Mosconi, F. De Angelis, *Sci. Rep.* **2014,***4*, 4467.
[27] C.J. Bartel, C. Sutton, B.R. Goldsmith, R. Ouyang, C.B. Musgrave, L.M. Ghiringhelli, M. Scheffler, *Sci. Adv.* **2019,***5*, eaav0693.
[28] M.M. Lee, J. Teuscher, T. Miyasaka, T.N. Murakami, H.J. Snaith, *Science* **2012,***338*, 643.
[29] D. Zhou, T. Zhou, Y. Tian, X. Zhu, Y. Tu, *J. Nanomater.* **2018,***2018*, 8148072.
[30] J.M. Ball, M.M. Lee, A. Hey, H.J. Snaith, *Energy Environ. Sci.* **2013,***6*, 1739.
[31] T. Miyasaka, *Chem. Lett.* **2015,***44*, 720.
[32] S. Zuo, X. Zhu, J. Feng, Z. Wang, C. Zhang, C. Wang, X. Ren, S. Liu, D. Yang, *Solar RRL* **2019,***3*, 1900207.
[33] C. Kuang, G. Tang, T. Jiu, H. Yang, H. Liu, B. Li, W. Luo, X. Li, W. Zhang, F. Lu, J. Fang, Y. Li, *Nano Lett.* **2015,***15*, 2756.
[34] D. Yang, X. Zhang, K. Wang, C. Wu, R. Yang, Y. Hou, Y. Jiang, S. Liu, S. Priya, *Nano Lett.* **2019,***19*, 3313.
[35] J. You, L. Meng, T.-B. Song, T.-F. Guo, Y. Yang, W.-H. Chang, Z. Hong, H. Chen, H. Zhou, Q. Chen, Y. Liu, N. De Marco, Y. Yang, *Nat. Nanotechnol.* **2016,***11*, 75.
[36] J. Song, G. Li, D. Wang, W. Sun, J. Wu, Z. Lan, *Solar RRL* **2020,***4*, 1900558.
[37] Q. Li, X. Zou, Y. Li, Y. Pei, S. Zeng, D. Guo, *Int. J. Photoenergy* **2017,***2017*, 8107073.
[38] L.-C. Chen, Z.-L. Tseng, J.-K. Huang, C.-C. Chen, S.H. Chang, *Coatings* **2016,***6*, 53.
[39] Y. Rong, Y. Hu, S. Ravishankar, H. Liu, X. Hou, Y. Sheng, A. Mei, Q. Wang, D. Li, M. Xu, J. Bisquert, H. Han, *Energy Environ. Sci.* **2017,***10*, 2383.
[40] J. Jiang, Q. Wang, Z. Jin, X. Zhang, J. Lei, H. Bin, Z.-G. Zhang, Y. Li, S. Liu, *Adv. Energy Mater.* **2018,***8*, 1701757.
[41] S.N. Habisreutinger, N.K. Noel, H.J. Snaith, *ACS Energy Lett.* **2018,***3*, 2472.
[42] Y.-L. Zhao, J.-F. Wang, B.-G. Zhao, C.-C. Jia, J.-P. Mou, L. Zhu, J. Song, X.-Q. Gu, Y.-H. Qiang, *Chin. Phys. B* **2018,***27*, 024208.
[43] Y. Chen, J. Shi, X. Li, S. Li, X. Lv, X. Sun, Y.-Z. Zheng, X. Tao, *J. Mater. Chem. A* **2020,***8*, 6349.
[44] R. Sedighi, F. Tajabadi, S. Shahbazi, S. Gholipour, N. Taghavinia, *ChemPhysChem* **2016,***17*, 2382.
[45] W. Ke, C. Xiao, C. Wang, B. Saparov, H.-S. Duan, D. Zhao, Z. Xiao, P. Schulz, S.P. Harvey, W. Liao, W. Meng, Y. Yu, A.J. Cimaroli, C.-S. Jiang, K. Zhu, M. Al-Jassim, G. Fang, D.B. Mitzi, Y. Yan, *Adv. Mater.* **2016,***28*, 5214.
[46] N. Mohammadian, A. Moshaii, A. Alizadeh, S. Gharibzadeh, R. Mohammadpour, *J. Phys. Chem. Lett.* **2016,***7*, 4614.
[47] A.-N. Cho, I.-H. Jang, J.-Y. Seo, N.-G. Park, *J. Mater. Chem. A* **2018,***6*, 18206.
[48] A.K. Jena, A. Kulkarni, M. Ikegami, T. Miyasaka, *J. Power Sources* **2016,***309*, 1.
[49] C. Liu, J. Fan, X. Zhang, Y. Shen, L. Yang, Y. Mai, *ACS Appl. Mater. Interfaces* **2015,***7*, 9066.
[50] H.-S. Kim, N.-G. Park, *J. Phys. Chem. Lett.* **2014,***5*, 2927.
[51] T. Leijtens, B. Lauber, G.E. Eperon, S.D. Stranks, H.J. Snaith, *J. Phys. Chem. Lett.* **2014,***5*, 1096.
[52] K.-M. Lee, W.-J. Lin, S.-H. Chen, M.-C. Wu, *Org. Electron.* **2020,***77*, 105406.
[53] J.P. Correa Baena, L. Steier, W. Tress, M. Saliba, S. Neutzner, T. Matsui, F. Giordano, T.J. Jacobsson, A.R. Srimath Kandada, S.M. Zakeeruddin, A. Petrozza, A. Abate, M.K. Nazeeruddin, M. Grätzel, A. Hagfeldt, *Energy Environ. Sci.* **2015,***8*, 2928.

[54] G. Namkoong, A.A. Mamun, T.T. Ava, *Org. Electron.* **2018,***56*, 163.
[55] J.H. Lee, I.S. Jin, Y.W. Noh, S.H. Park, J.W. Jung, *ACS Sustainable Chem. Eng.* **2019,***7*, 17661.
[56] H. Rao, W. Sun, S. Ye, W. Yan, Y. Li, H. Peng, Z. Liu, Z. Bian, C. Huang, *ACS Appl. Mater. Interfaces* **2016,***8*, 7800.
[57] Z. Liu, Q. Chen, J.-W. Lee, Z. Zhao, X. Xu, Y.-T. Hsieh, L. Meng, P. Sun, N.D. Marco, H. Zhou, Y.-B. Cheng, Y. Yang, *Adv. Energy Mater.* **2018,***8*, 1800568.
[58] C. Wang, C. Zhang, Y. Huang, S. Tong, H. Wu, J. Zhang, Y. Gao, J. Yang, *Synth. Met.* **2017,***227*, 43.
[59] Q. Jiang, L. Zhang, H. Wang, X. Yang, J. Meng, H. Liu, Z. Yin, J. Wu, X. Zhang, J. You, *Nat. Energy* **2016,***2*, 16177.
[60] Q. Zhu, Z. Wang, X. Cai, W. Wang, G. Wu, L. Kong, X. Zheng, Y. Cao, Y. Wu, X. Li, Z. Wu, J. Kang, *J. Power Sources* **2020,***465*, 228251.
[61] W. Chen, X. Yin, M. Que, H. Xie, J. Liu, C. Yang, Y. Guo, Y. Wu, W. Que, *J. Power Sources* **2019,***412*, 118.
[62] J.H. Heo, H.J. Han, D. Kim, T.K. Ahn, S.H. Im, *Energy Environ. Sci.* **2015,***8*, 1602.
[63] H. Gu, C. Zhao, Y. Zhang, G. Shao, *Nanotechnology* **2018,***29*, 385401.
[64] F. Wu, B. Bahrami, K. Chen, S. Mabrouk, R. Pathak, Y. Tong, X. Li, T. Zhang, R. Jian, Q. Qiao, *ACS Appl. Mater. Interfaces* **2018,***10*, 25604.
[65] W. Tress, N. Marinova, T. Moehl, S.M. Zakeeruddin, M.K. Nazeeruddin, M. Grätzel, *Energy Environ. Sci.* **2015,***8*, 995.
[66] J.H. Lee, Y.W. Noh, I.S. Jin, S.H. Park, J.W. Jung, *J. Mater. Chem. C.* **2019,***7*, 7288.
[67] J. Wei, Y. Zhao, H. Li, G. Li, J. Pan, D. Xu, Q. Zhao, D. Yu, *J. Phys. Chem. Lett.* **2014,***5*, 3937.
[68] Y. Jiang, Y. Feng, X. Sun, R. Qin, H. Ma, *J. Phys. D: Appl. Phys.* **2019,***52*, 385501.
[69] C. Xia, W.-D. Song, C.-Z. Zhang, S.-Y. Yuan, W.-X. Hu, P. Qin, R.-P. Wang, L.-L. Zhao, X.-F. Wang, M. He, S.-T. Li, *Chin. Phys. B* **2017,***26*, 018401.
[70] L.K. Ono, S.R. Raga, S. Wang, Y. Kato, Y. Qi, *J. Mater. Chem. A* **2015,***3*, 9074.
[71] L. Yang, B. Xu, D. Bi, H. Tian, G. Boschloo, L. Sun, A. Hagfeldt, E.M.J. Johansson, *J. Am. Chem. Soc.* **2013,***135*, 7378.
[72] C. Zhao, B. Chen, X. Qiao, L. Luan, K. Lu, B. Hu, *Adv. Energy Mater.* **2015,***5*, 1500279.
[73] G. Liu, B. Yang, B. Liu, C. Zhang, S. Xiao, Y. Yuan, H. Xie, D. Niu, J. Yang, Y. Gao, C. Zhou, *Appl. Phys. Lett.* **2017,***111*, 153501
[74] Q. Wang, X. Zhang, Z. Jin, J. Zhang, Z. Gao, Y. Li, S. Liu, *ACS Energy Lett.* **2017,***2*, 1479.
[75] X. Deng, X. Wen, J. Zheng, T. Young, C.F.J. Lau, J. Kim, M. Green, S. Huang, A. Ho-Baillie, *Nano Energy* **2018,***46*, 356.
[76] X. Wu, J. Wang, E.K.L. Yeow, *J. Phys. Chem. C.* **2016,***120*, 12273.
[77] C. Yang, Z. Hu, C. Gao, Y. Wang, H. Zhang, J. Wang, J. Zhang, X. Zhou, Y. Zhu, *J. Phys. Chem. C.* **2020,***124*, 1851.
[78] J. Xiao, J. Chang, B. Li, F.H. Isikgor, D. Wang, Z. Fan, Z. Lin, J. Ouyang, K. Zeng, J. Chen, *J. Mater. Chem. A* **2018,***6*, 9665.
[79] Y. Liu, L. Collins, R. Proksch, S. Kim, B.R. Watson, B. Doughty, T.R. Calhoun, M. Ahmadi, A.V. Ievlev, S. Jesse, S.T. Retterer, A. Belianinov, K. Xiao, J. Huang, B.G. Sumpter, S.V. Kalinin, B. Hu, O.S. Ovchinnikova, *Nat. Mater.* **2018,***17*, 1013.
[80] A. Gómez, Q. Wang, A.R. Goñi, M. Campoy-Quiles, A. Abate, *Energy Environ. Sci.* **2019,***12*, 2537.

[81] B. Chen, X. Zheng, M. Yang, Y. Zhou, S. Kundu, J. Shi, K. Zhu, S. Priya, *Nano Energy* **2015,***13*, 582.

[82] H.-W. Chen, N. Sakai, M. Ikegami, T. Miyasaka, *J. Phys. Chem. Lett.* **2015,***6*, 164.

[83] G.E. Eperon, G.M. Paternò, R.J. Sutton, A. Zampetti, A.A. Haghighirad, F. Cacialli, H.J. Snaith, *J. Mater. Chem. A* **2015,***3*, 19688.

[84] S. Meloni, T. Moehl, W. Tress, M. Franckevičius, M. Saliba, Y.H. Lee, P. Gao, M.K. Nazeeruddin, S.M. Zakeeruddin, U. Rothlisberger, M. Graetzel, *Nat. Commun.* **2016,***7*, 10334.

[85] E. Edri, S. Kirmayer, A. Henning, S. Mukhopadhyay, K. Gartsman, Y. Rosenwaks, G. Hodes, D. Cahen, *Nano Lett.* **2014,***14*, 1000.

[86] D. Yang, R. Yang, K. Wang, C. Wu, X. Zhu, J. Feng, X. Ren, G. Fang, S. Priya, S. Liu, *Nat. Commun.* **2018,***9*, 3239.

[87] F. Arabpour Roghabadi, N. Mansour Rezaei Fumani, M. Alidaei, V. Ahmadi, S.M. Sadrameli, *Sci. Rep.* **2019,***9*, 9448.

[88] M.F. Aygüler, A.G. Hufnagel, P. Rieder, M. Wussler, W. Jaegermann, T. Bein, V. Dyakonov, M.L. Petrus, A. Baumann, P. Docampo, *ACS Appl. Mater. Interfaces* **2018,***10*, 11414.

[89] R. Zhang, M. Li, Y. Huan, J. Xi, S. Zhang, X. Cheng, H. Wu, W. Peng, Z. Bai, X. Yan, *Inorg. Chem. Front.* **2019,***6*, 434.

[90] J. Mizusaki, K. Arai, K. Fueki, *Solid State Ionics* **1983,***11*, 203.

[91] Y. Yuan, J. Huang, *Acc. Chem. Res.* **2016,***49*, 286.

[92] R. García-Rodríguez, D. Ferdani, S. Pering, P.J. Baker, P.J. Cameron, *J. Mater. Chem. A* **2019,***7*, 22604.

[93] Y. Yuan, J. Chae, Y. Shao, Q. Wang, Z. Xiao, A. Centrone, J. Huang, *Adv. Energy Mater.* **2015,***5*, 1500615.

[94] Y. Liu, A.V. Ievlev, L. Collins, N. Borodinov, A. Belianinov, J.K. Keum, M. Wang, M. Ahmadi, S. Jesse, K. Xiao, B.G. Sumpter, B. Hu, S.V. Kalinin, O.S. Ovchinnikova, *Adv. Opt. Mater.* **2019,***7*, 1901451.

[95] Y. Liu, M. Lorenz, A.V. Ievlev, O.S. Ovchinnikova, *Adv. Funct. Mater.* **2020,***30*, 2002201.

[96] Y.-C. Zhao, W.-K. Zhou, X. Zhou, K.-H. Liu, D.-P. Yu, Q. Zhao, *Light: Sci. Appl.* **2017,***6*, e16243.

[97] J.-F. Wang, D.-X. Lin, Y.-B. Yuan, *Acta. Phys. Sin.* **2019,***68*, 158801.

[98] D.A. Egger, L. Kronik, A.M. Rappe, *Angew. Chem. Int. Ed.* **2015,***54*, 12437.

[99] J. Kim, S.-H. Lee, J.H. Lee, K.-H. Hong, *J. Phys. Chem. Lett.* **2014,***5*, 1312.

[100] C. Eames, J.M. Frost, P.R.F. Barnes, B.C. O'Regan, A. Walsh, M.S. Islam, *Nat. Commun.* **2015,***6*, 7497.

[101] J.M. Azpiroz, E. Mosconi, J. Bisquert, F. De Angelis, *Energy Environ. Sci.* **2015,***8*, 2118.

[102] Y. Liu, N. Borodinov, M. Lorenz, M. Ahmadi, S.V. Kalinin, A.V. Ievlev, O.S. Ovchinnikova, *Adv. Sci.* **2020,***7*, 2001176.

[103] M.H. Futscher, J.M. Lee, L. McGovern, L.A. Muscarella, T. Wang, M.I. Haider, A. Fakharuddin, L. Schmidt-Mende, B. Ehrler, *Mater. Horiz.* **2019,***6*, 1497.

[104] O. Almora, I. Zarazua, E. Mas-Marza, I. Mora-Sero, J. Bisquert, G. Garcia-Belmonte, *J. Phys. Chem. Lett.* **2015,***6*, 1645.

[105] B. Chen, M. Yang, X. Zheng, C. Wu, W. Li, Y. Yan, J. Bisquert, G. Garcia-Belmonte, K. Zhu, S. Priya, *J. Phys. Chem. Lett.* **2015,***6*, 4693.

[106] B. Chen, M. Yang, S. Priya, K. Zhu, *J. Phys. Chem. Lett.* **2016,***7*, 905.

[107] R.S. Sanchez, V. Gonzalez-Pedro, J.-W. Lee, N.-G. Park, Y.S. Kang, I. Mora-Sero, J. Bisquert, *J.*

Phys. Chem. Lett. **2014,***5*, 2357.
[108] D.A. Jacobs, Y. Wu, H. Shen, C. Barugkin, F.J. Beck, T.P. White, K. Weber, K.R. Catchpole, *Phys. Chem. Chem. Phys.* **2017,***19*, 3094.
[109] T.W. Kim, M. Kim, L. Cojocaru, S. Uchida, H. Segawa, *ACS Energy Lett.* **2018,***3*, 2743.
[110] A. Pockett, G.E. Eperon, N. Sakai, H.J. Snaith, L.M. Peter, P.J. Cameron, *Phys. Chem. Chem. Phys.* **2017,***19*, 5959.
[111] A.M.A. Leguy, J.M. Frost, A.P. McMahon, V.G. Sakai, W. Kockelmann, C. Law, X. Li, F. Foglia, A. Walsh, B.C. O'Regan, J. Nelson, J.T. Cabral, P.R.F. Barnes, *Nat. Commun.* **2015,***6*, 7124.
[112] S. van Reenen, M. Kemerink, H.J. Snaith, *J. Phys. Chem. Lett.* **2015,***6*, 3808.
[113] N.D. Pham, C. Zhang, V.T. Tiong, S. Zhang, G. Will, A. Bou, J. Bisquert, P.E. Shaw, A. Du, G.J. Wilson, H. Wang, *Adv. Funct. Mater.* **2019,***29*, 1806479.
[114] T. Bu, X. Liu, Y. Zhou, J. Yi, X. Huang, L. Luo, J. Xiao, Z. Ku, Y. Peng, F. Huang, Y.-B. Cheng, J. Zhong, *Energy Environ. Sci.* **2017,***10*, 2509.
[115] T. Bu, X. Liu, J. Li, W. Li, W. Huang, Z. Ku, Y. Peng, F. Huang, Y.-B. Cheng, J. Zhong, *Electrochim. Acta* **2019,***306*, 635.
[116] C. Yi, J. Luo, S. Meloni, A. Boziki, N. Ashari-Astani, C. Grätzel, S.M. Zakeeruddin, U. Röthlisberger, M. Grätzel, *Energy Environ. Sci.* **2016,***9*, 656.
[117] H. Fu, *Sol. Energy Mater. Sol. Cells* **2019,***193*, 107.
[118] Y. Zong, N. Wang, L. Zhang, M.-G. Ju, X.C. Zeng, X.W. Sun, Y. Zhou, N.P. Padture, *Angew. Chem. Int. Ed.* **2017,***56*, 12658.
[119] Y. Wang, W. Fu, J. Yan, J. Chen, W. Yang, H. Chen, *J. Mater. Chem. A* **2018,***6*, 13090.
[120] X. Ge, X. Qu, L. He, Y. Sun, X. Guan, Z. Pang, C. Wang, L. Yang, F. Wang, F. Rosei, *J. Mater. Chem. A* **2019,***7*, 27225.
[121] C.-G. Wu, C.-H. Chiang, Z.-L. Tseng, M.K. Nazeeruddin, A. Hagfeldt, M. Grätzel, *Energy Environ. Sci.* **2015,***8*, 2725.
[122] H. Chen, T. Liu, P. Zhou, S. Li, J. Ren, H. He, J. Wang, N. Wang, S. Guo, *Adv. Mater.* **2020,***32*, 1905661.
[123] X. Yan, S. Hu, Y. Zhang, H. Li, C. Sheng, *Sol. Energy Mater. Sol. Cells* **2019,***191*, 283.
[124] J. Yan, S. Lin, X. Qiu, H. Chen, K. Li, Y. Yuan, M. Long, B. Yang, Y. Gao, C. Zhou, *Appl. Phys. Lett.* **2019,***114*, 103503.
[125] C.-H. Chiang, M.K. Nazeeruddin, M. Grätzel, C.-G. Wu, *Energy Environ. Sci.* **2017,***10*, 808.
[126] S. Jin, Y. Wei, X. Yang, D. Luo, Y. Fang, Y. Zhao, Q. Guo, Y. Huang, L. Fan, J. Wu, *Org. Electron.* **2018,***63*, 207.
[127] H. Jiang, G. Jiang, W. Xing, W. Xiong, X. Zhang, B. Wang, H. Zhang, Y. Zheng, *ACS Appl. Mater. Interfaces* **2018,***10*, 29954.
[128] F. Wu, T. Chen, X. Yue, L. Zhu, *Org. Electron.* **2018,***58*, 6.
[129] Y.-H. Seo, E.-C. Kim, S.-P. Cho, S.-S. Kim, S.-I. Na, *Appl. Mater. Today* **2017,***9*, 598.
[130] Y. Rong, Z. Tang, Y. Zhao, X. Zhong, S. Venkatesan, H. Graham, M. Patton, Y. Jing, A.M. Guloy, Y. Yao, *Nanoscale* **2015,***7*, 10595.
[131] L. Chao, Y. Xia, B. Li, G. Xing, Y. Chen, W. Huang, *Chem.* **2019,***5*, 995.
[132] Z. Liu, L. Wang, J. Han, F. Zeng, G. Liu, X. Xie, *Org. Electron.* **2020,***78*, 105552.
[133] Y.-Q. Zhao, Q.-R. Ma, B. Liu, Z.-L. Yu, J. Yang, M.-Q. Cai, *Nanoscale* **2018,***10*, 8677.
[134] S.-Q. Luo, J.-F. Wang, B. Yang, Y.-B. Yuan, *Front. Phys.* **2019,***14*, 53401.
[135] K. Wang, Z. Li, F. Zhou, H. Wang, H. Bian, H. Zhang, Q. Wang, Z. Jin, L. Ding, S. Liu, *Adv.*

Energy Mater. **2019,***9*, 1902529.
[136] Y. Xu, M. Wang, Y. Lei, Z. Ci, Z. Jin, *Adv. Energy Mater.* **2020**, DOI: 10.1002/aenm.202002558.
[137] H. Tsai, W. Nie, J.-C. Blancon, C.C. Stoumpos, R. Asadpour, B. Harutyunyan, A.J. Neukirch, R. Verduzco, J.J. Crochet, S. Tretiak, L. Pedesseau, J. Even, M.A. Alam, G. Gupta, J. Lou, P.M. Ajayan, M.J. Bedzyk, M.G. Kanatzidis, A.D. Mohite, *Nature* **2016,***536*, 312.
[138] L.N. Quan, M. Yuan, R. Comin, O. Voznyy, E.M. Beauregard, S. Hoogland, A. Buin, A.R. Kirmani, K. Zhao, A. Amassian, D.H. Kim, E.H. Sargent, *J. Am. Chem. Soc.* **2016,***138*, 2649.
[139] H. Lai, B. Kan, T. Liu, N. Zheng, Z. Xie, T. Zhou, X. Wan, X. Zhang, Y. Liu, Y. Chen, *J. Am. Chem. Soc.* **2018,***140*, 11639.
[140] J. Zhang, J. Qin, M. Wang, Y. Bai, H. Zou, J.K. Keum, R. Tao, H. Xu, H. Yu, S. Haacke, B. Hu, *Joule* **2019,***3*, 3061.
[141] S. Shao, H. Duim, Q. Wang, B. Xu, J. Dong, S. Adjokatse, G.R. Blake, L. Protesescu, G. Portale, J. Hou, M. Saba, M.A. Loi, *ACS Energy Lett.* **2020,***5*, 39.
[142] P. Li, X. Liu, Y. Zhang, C. Liang, G. Chen, F. Li, M. Su, G. Xing, X. Tao, Y. Song, *Angew. Chem. Int. Ed.* **2020,***59*, 6909.
[143] P. Li, C. Liang, X.-L. Liu, F. Li, Y. Zhang, X.-T. Liu, H. Gu, X. Hu, G. Xing, X. Tao, Y. Song, *Adv. Mater.* **2019,***31*, 1901966.
[144] H. Wang, H. Bian, Z. Jin, L. Liang, D. Bai, Q. Wang, S. Liu, *Solar RRL* **2018,***2*, 1800216.
[145] Z. Wang, Q. Lin, F.P. Chmiel, N. Sakai, L.M. Herz, H.J. Snaith, *Nat. Energy* **2017,***2*, 17135.
[146] S. Shao, J. Liu, G. Portale, H.-H. Fang, G.R. Blake, G.H. ten Brink, L.J.A. Koster, M.A. Loi, *Adv. Energy Mater.* **2018,***8*, 1702019.
[147] Z. Zhou, L. Huang, X. Mei, Y. Zhao, Z. Lin, H. Zhen, Q. Ling, *Solar Energy* **2016,***136*, 210.
[148] K. Wang, L. Zheng, T. Zhu, L. Liu, M.L. Becker, X. Gong, *Nano Energy* **2020,***67*, 104229.
[149] R. Singh, S. Sandhu, H. Yadav, J.-J. Lee, *ACS Appl. Mater. Interfaces* **2019,***11*, 29941.
[150] X. Li, D. Bi, C. Yi, J.-D. Décoppet, J. Luo, S.M. Zakeeruddin, A. Hagfeldt, M. Grätzel, *Science* **2016,***353*, 58.
[151] T. Gotanda, H. Oooka, S. Mori, H. Nakao, A. Amano, K. Todori, Y. Nakai, K. Mizuguchi, *J. Power Sources* **2019,***430*, 145.
[152] J. Duan, Y. Zhang, D. Yu, F. Wang, J. Dai, *ChemNanoMat* **2019,***5*, 715.
[153] Y. Yang, S. Feng, W. Xu, M. Li, L. Li, X. Zhang, G. Ji, X. Zhang, Z. Wang, Y. Xiong, L. Cao, B. Sun, X. Gao, *ACS Appl. Mater. Interfaces* **2017,***9*, 23141.
[154] W. Nie, H. Tsai, R. Asadpour, J.-C. Blancon, A.J. Neukirch, G. Gupta, J.J. Crochet, M. Chhowalla, S. Tretiak, M.A. Alam, H.-L. Wang, A.D. Mohite, *Science* **2015,***347*, 522.
[155] J.J. van Franeker, K.H. Hendriks, B.J. Bruijnaers, M.W.G.M. Verhoeven, M.M. Wienk, R.A.J. Janssen, *Adv. Energy Mater.* **2017,***7*, 1601822.
[156] Y. Wu, X. Yang, W. Chen, Y. Yue, M. Cai, F. Xie, E. Bi, A. Islam, L. Han, *Nat. Energy* **2016,***1*, 16148.
[157] J. Zhang, D. Bai, Z. Jin, H. Bian, K. Wang, J. Sun, Q. Wang, S. Liu, *Adv. Energy Mater.* **2018,***8*, 1703246.
[158] Z. Chen, G. Yang, X. Zheng, H. Lei, C. Chen, J. Ma, H. Wang, G. Fang, *J. Power Sources* **2017,***351*, 123.
[159] J. Zhen, W. Zhou, M. Chen, B. Li, L. Jia, M. Wang, S. Yang, *J. Mater. Chem. A* **2019,***7*, 2754.
[160] R. Singh, V.K. Shukla, *Solar Energy* **2019,***178*, 90.
[161] W. Xu, L. Zheng, T. Zhu, L. Liu, X. Gong, *ACS Appl. Mater. Interfaces* **2019,***11*, 34020.

[162] A. Rajagopal, P.-W. Liang, C.-C. Chueh, Z. Yang, A.K.Y. Jen, *ACS Energy Lett.* **2017,***2*, 2531.
[163] H. Bian, D. Bai, Z. Jin, K. Wang, L. Liang, H. Wang, J. Zhang, Q. Wang, S. Liu, *Joule* **2018,***2*, 1500.
[164] K. Wang, Z. Jin, L. Liang, H. Bian, D. Bai, H. Wang, J. Zhang, Q. Wang, S. Liu, *Nat. Commun.* **2018,***9*, 4544.
[165] J.H. Heo, M.S. You, M.H. Chang, W. Yin, T.K. Ahn, S.-J. Lee, S.-J. Sung, D.H. Kim, S.H. Im, *Nano Energy* **2015,***15*, 530.
[166] J. Song, S.P. Li, Y.L. Zhao, J. Yuan, Y. Zhu, Y. Fang, L. Zhu, X.Q. Gu, Y.H. Qiang, *J. Alloys Comp.* **2017,***694*, 1232.
[167] C. Liang, P. Li, Y. Zhang, H. Gu, Q. Cai, X. Liu, J. Wang, H. Wen, G. Shao, *J. Power Sources* **2017,***372*, 235.
[168] L.-L. Jiang, Z.-K. Wang, M. Li, C.-H. Li, P.-F. Fang, L.-S. Liao, *Solar RRL* **2018,***2*, 1800149.
[169] S. Wang, B. Liu, Y. Zhu, Z. Ma, B. Liu, X. Miao, R. Ma, C. Wang, *Solar Energy* **2018,***169*, 335.
[170] X. Ren, L. Xie, W.B. Kim, D.G. Lee, H.S. Jung, S. Liu, *Solar RRL* **2019,***3*, 1900176.
[171] J.Y. Kim, S. Rhee, H. Lee, K. An, S. Biswas, Y. Lee, J.W. Shim, C. Lee, H. Kim, *Adv. Mater. Interfaces* **2020,***7*, 1902003.
[172] R.D. Chavan, P. Yadav, A. Nimbalkar, S.P. Bhoite, P.N. Bhosale, C. Kook Hong, *Solar Energy* **2019,***186*, 156.
[173] F. Yu, G.S. Han, Y.J. Tu, H.-S. Roh, J.-K. Lee, *Solar Energy* **2018,***167*, 251.
[174] Y. Yu, J. Li, D. Geng, J. Wang, L. Zhang, T.L. Andrew, M.S. Arnold, X. Wang, *ACS Nano* **2015,***9*, 564.
[175] Y. Gao, Y. Dong, K. Huang, C. Zhang, B. Liu, S. Wang, J. Shi, H. Xie, H. Huang, S. Xiao, J. He, Y. Gao, R.A. Hatton, J. Yang, *ACS Photon.* **2018,***5*, 4104.
[176] J.H. Heo, M.H. Lee, H.J. Han, B.R. Patil, J.S. Yu, S.H. Im, *J. Mater. Chem. A* **2016,***4*, 1572.
[177] W. Hu, T. Liu, X. Yin, H. Liu, X. Zhao, S. Luo, Y. Guo, Z. Yao, J. Wang, N. Wang, H. Lin, Z. Guo, *J. Mater. Chem. A* **2017,***5*, 1434.
[178] W.-Q. Wu, D. Chen, F. Li, Y.-B. Cheng, R.A. Caruso, *Mater. Today Energy* **2018,***7*, 260.
[179] X. Li, J. Yang, Q. Jiang, H. Lai, S. Li, J. Xin, W. Chu, J. Hou, *ACS Nano* **2018,***12*, 5605.
[180] N. Tsvetkov, B.C. Moon, J.Y. Lee, J.K. Kang, *ACS Appl. Energy Mater.* **2020,***3*, 344.
[181] X. Liu, Z. Liu, H. Ye, Y. Tu, B. Sun, X. Tan, T. Shi, Z. Tang, G. Liao, *Electrochim. Acta* **2018,***288*, 115.
[182] Y. Zheng, J. Kong, D. Huang, W. Shi, L. McMillon-Brown, H.E. Katz, J. Yu, A.D. Taylor, *Nanoscale* **2018,***10*, 11342.
[183] X. Meng, J. Zhou, J. Hou, X. Tao, S.H. Cheung, S.K. So, S. Yang, *Adv. Mater.* **2018,***30*, 1706975.
[184] M.B. Upama, N.K. Elumalai, M.A. Mahmud, D. Wang, F. Haque, V.R. Gonçales, J.J. Gooding, M. Wright, C. Xu, A. Uddin, *Org. Electron.* **2017,***50*, 279.
[185] J. Huang, X. Yu, J. Xie, C.-Z. Li, Y. Zhang, D. Xu, Z. Tang, C. Cui, D. Yang, *ACS Appl. Mater. Interfaces* **2016,***8*, 34612.
[186] L. Zhao, X. Wang, X. Li, W. Zhang, X. Liu, Y. Zhu, H.-Q. Wang, J. Fang, *Sol. Energy Mater. Sol. Cells* **2016,***157*, 79.
[187] Z. Zhu, J.-Q. Xu, C.-C. Chueh, H. Liu, Z.a. Li, X. Li, H. Chen, A.K.Y. Jen, *Adv. Mater.* **2016,***28*, 10786.
[188] B. Fan, Z. He, J. Xiong, Q. Zhao, Z. Dai, B. Yang, X. Xue, P. Cai, S. Zhan, S. Tong, J. Yang, J. Zhang, *Solar Energy* **2019,***189*, 307.

[189] D. Yang, R. Yang, X. Ren, X. Zhu, Z. Yang, C. Li, S. Liu, *Adv. Mater.* **2016,***28*, 5206.
[190] Z. Ma, W. Zhou, Z. Xiao, H. Zhang, Z. Li, J. Zhuang, C. Peng, Y. Huang, *Org. Electron.* **2019,***71*, 98.
[191] G. Yang, H. Lei, H. Tao, X. Zheng, J. Ma, Q. Liu, W. Ke, Z. Chen, L. Xiong, P. Qin, Z. Chen, M. Qin, X. Lu, Y. Yan, G. Fang, *Small* **2017,***13*, 1601769.
[192] J. Chen, H. Dong, L. Zhang, J. Li, F. Jia, B. Jiao, J. Xu, X. Hou, J. Liu, Z. Wu, *J. Mater. Chem. A* **2020,***8*, 2644.
[193] Z. Zhu, Q. Xue, H. He, K. Jiang, Z. Hu, Y. Bai, T. Zhang, S. Xiao, K. Gundogdu, B.R. Gautam, H. Ade, F. Huang, K.S. Wong, H.-L. Yip, S. Yang, H. Yan, *Adv. Sci.* **2016,***3*, 1500353.
[194] K. Mahmood, A. Khalid, S.W. Ahmad, M.T. Mehran, *Surf. Coat. Technol.* **2018,***352*, 231.
[195] K. Mahmood, A. Khalid, *Mater. Lett.* **2018,***224*, 78.
[196] Y.-N. Zhang, B. Li, L. Fu, Q. Li, L.-W. Yin, *Electrochim. Acta* **2020,***330*, 135280.
[197] Y. Chen, C. Xu, J. Xiong, Z. Zhang, X. Zhang, J. Yang, X. Xue, D. Yang, J. Zhang, *Org. Electron.* **2018,***58*, 294.
[198] H. Dong, S. Pang, Y. Zhang, D. Chen, W. Zhu, H. Xi, J. Chang, J. Zhang, C. Zhang, Y. Hao, *Nanomaterials* **2018,***8*, 720.
[199] F. Rehman, K. Mahmood, A. Khalid, M.S. Zafar, M. Hameed, *J. Colloid Interface Sci.* **2019,***535*, 353.
[200] A.S. Subbiah, A.K. Dhara, N. Mahuli, S. Banerjee, S.K. Sarkar, *Energy Technol.* **2020,***8*, 1900878.
[201] C. Liu, M. Cai, Y. Yang, Z. Arain, Y. Ding, X. Shi, P. Shi, S. Ma, T. Hayat, A. Alsaedi, J. Wu, S. Dai, G. Cao, *J. Mater. Chem. A* **2019,***7*, 11086.
[202] C. Huang, P. Lin, N. Fu, C. Liu, B. Xu, K. Sun, D. Wang, X. Zeng, S. Ke, *Chem. Commun.* **2019,***55*, 2777.
[203] J.-F. Liao, W.-Q. Wu, Y. Jiang, D.-B. Kuang, L. Wang, *Solar RRL* **2019,***3*, 1800268.
[204] L. Liang, M. Liu, Z. Jin, Q. Wang, H. Wang, H. Bian, F. Shi, S. Liu, *Nano Lett.* **2019,***19*, 1796.
[205] H. Xi, S. Tang, X. Ma, J. Chang, D. Chen, Z. Lin, P. Zhong, H. Wang, C. Zhang, *ACS Omega* **2017,***2*, 326.
[206] S. Wang, W. Yuan, Y.S. Meng, *ACS Appl. Mater. Interfaces* **2015,***7*, 24791.
[207] L.-L. Jiang, Z.-K. Wang, M. Li, C.-H. Li, P.-F. Fang, L.-S. Liao, *J. Mater. Chem. A* **2019,***7*, 3655.
[208] W. Li, H. Dong, L. Wang, N. Li, X. Guo, J. Li, Y. Qiu, *J. Mater. Chem. A* **2014,***2*, 13587.
[209] J. Luo, C. Jia, Z. Wan, F. Han, B. Zhao, R. Wang, *J. Power Sources* **2017,***342*, 886.
[210] J. Zou, J. Wu, W. Sun, M. Zhang, X. Wang, P. Yuan, Q. Zhu, J. Yin, X. Liu, Y. Yang, *Solar Energy* **2019,***194*, 321.
[211] M. Jeong, I.W. Choi, E.M. Go, Y. Cho, M. Kim, B. Lee, S. Jeong, Y. Jo, H.W. Choi, J. Lee, J.-H. Bae, S.K. Kwak, D.S. Kim, C. Yang, *Science* **2020,***369*, 1615.
[212] D. Bai, J. Zhang, Z. Jin, H. Bian, K. Wang, H. Wang, L. Liang, Q. Wang, S. Liu, *ACS Energy Lett.* **2018,***3*, 970.
[213] Q. Zhao, R. Wu, Z. Zhang, J. Xiong, Z. He, B. Fan, Z. Dai, B. Yang, X. Xue, P. Cai, S. Zhan, X. Zhang, J. Zhang, *Org. Electron.* **2019,***71*, 106.
[214] C. Wang, C. Zhang, S. Tong, H. Xia, L. Wang, H. Xie, Y. Gao, J. Yang, *J. Phys. D: Appl. Phys.* **2018,***51*, 025110.
[215] E.H. Jung, N.J. Jeon, E.Y. Park, C.S. Moon, T.J. Shin, T.-Y. Yang, J.H. Noh, J. Seo, *Nature* **2019,***567*, 511.

[216] H.-W. Chen, T.-Y. Huang, T.-H. Chang, Y. Sanehira, C.-W. Kung, C.-W. Chu, M. Ikegami, T. Miyasaka, K.-C. Ho, *Sci. Rep.* **2016,***6*, 34319.

[217] R. Xue, M. Zhang, G. Xu, J. Zhang, W. Chen, H. Chen, M. Yang, C. Cui, Y. Li, Y. Li, *J. Mater. Chem. A* **2018,***6*, 404.

[218] W. Yu, F. Li, H. Wang, E. Alarousu, Y. Chen, B. Lin, L. Wang, M.N. Hedhili, Y. Li, K. Wu, X. Wang, O.F. Mohammed, T. Wu, *Nanoscale* **2016,***8*, 6173.

[219] D. Di Girolamo, F. Matteocci, F.U. Kosasih, G. Chistiakova, W. Zuo, G. Divitini, L. Korte, C. Ducati, A. Di Carlo, D. Dini, A. Abate, *Adv. Energy Mater.* **2019,***9*, 1901642.

[220] D. Ouyang, J. Xiao, F. Ye, Z. Huang, H. Zhang, L. Zhu, J. Cheng, W.C.H. Choy, *Adv. Energy Mater.* **2018,***8*, 1702722.

[221] G.A. Sepalage, S. Meyer, A.R. Pascoe, A.D. Scully, U. Bach, Y.-B. Cheng, L. Spiccia, *Nano Energy* **2017,***32*, 310.

[222] Y. Cao, H. Wu, W. Li, Z. Zhao, Z. Xiao, W. Zi, N. Cheng, J. Liu, Y. Tu, *Org. Electron.* **2020,***76*, 105455.

[223] T. Duong, J. Peng, D. Walter, J. Xiang, H. Shen, D. Chugh, M. Lockrey, D. Zhong, J. Li, K. Weber, T.P. White, K.R. Catchpole, *ACS Energy Lett.* **2018,***3*, 2441.

[224] W. Sun, Y. Li, S. Ye, H. Rao, W. Yan, H. Peng, Y. Li, Z. Liu, S. Wang, Z. Chen, L. Xiao, Z. Bian, C. Huang, *Nanoscale* **2016,***8*, 10806.

[225] J.W. Jung, C.-C. Chueh, A.K.Y. Jen, *Adv. Energy Mater.* **2015,***5*, 1500486.

[226] J. Luo, J. Xia, H. Yang, L. Chen, Z. Wan, F. Han, H.A. Malik, X. Zhu, C. Jia, *Energy Environ. Sci.* **2018,***11*, 2035.

[227] A.M. Oo, P. Fan, X. Zhang, J. Yu, *Energy Technol.* **2020,***8*, 1901042.

[228] Q. He, K. Yao, X. Wang, X. Xia, S. Leng, F. Li, *ACS Appl. Mater. Interfaces* **2017,***9*, 41887.

[229] T. Liu, J. Zhang, X. Wu, H. Liu, F. Li, X. Deng, F. Lin, X. Li, Z. Zhu, A.K.Y. Jen, *Solar RRL* **2020,***4*, 2000205.

[230] N.K. Noel, S.N. Habisreutinger, B. Wenger, Y.-H. Lin, F. Zhang, J.B. Patel, A. Kahn, M.B. Johnston, H.J. Snaith, *Adv. Energy Mater.* **2020,***10*, 1903231.

[231] W. Li, X. Lai, F. Meng, G. Li, K. Wang, A.K.K. Kyaw, X.W. Sun, *Sol. Energy Mater. Sol. Cells* **2020,***211*, 110527.

[232] X. Liu, K.-W. Tsai, Z. Zhu, Y. Sun, C.-C. Chueh, A.K.Y. Jen, *Adv. Mater. Interfaces* **2016,***3*, 1600122.

[233] Z. Gu, L. Zuo, T.T. Larsen-Olsen, T. Ye, G. Wu, F.C. Krebs, H. Chen, *J. Mater. Chem. A* **2015,***3*, 24254.

[234] H. Zhu, Y. Liu, F.T. Eickemeyer, L. Pan, D. Ren, M.A. Ruiz-Preciado, B. Carlsen, B. Yang, X. Dong, Z. Wang, H. Liu, S. Wang, S.M. Zakeeruddin, A. Hagfeldt, M.I. Dar, X. Li, M. Grätzel, *Adv. Mater.* **2020,***32*, 1907757.

[235] D. Zhang, H. Tian, S. Bu, T. Yan, J. Ge, T. Lei, W. Bi, L. Huang, Z. Ge, *J. Alloys Comp.* **2020,***831*, 154717.

[236] J. Dong, J. Jia, B. Cao, J. Lin, L. Fan, Z. Lan, J. Wu, *Org. Electron.* **2019,***75*, 105426.

[237] J. Cao, B. Wu, R. Chen, Y. Wu, Y. Hui, B.-W. Mao, N. Zheng, *Adv. Mater.* **2018,***30*, 1705596.

[238] Y. Li, Y. Zhao, Q. Chen, Y. Yang, Y. Liu, Z. Hong, Z. Liu, Y.-T. Hsieh, L. Meng, Y. Li, Y. Yang, *J. Am. Chem. Soc.* **2015,***137*, 15540.

[239] W. Chen, Y. Wu, J. Liu, C. Qin, X. Yang, A. Islam, Y.-B. Cheng, L. Han, *Energy Environ. Sci.* **2015,***8*, 629.

[240] Z. Li, C. Liu, G. Ren, W. Han, L. Shen, W. Guo, *Solar RRL* **2020,***4*, 1900369.
[241] J. Chen, J.-Y. Seo, N.-G. Park, *Adv. Energy Mater.* **2018,***8*, 1702714.
[242] M.A. Mahmud, T. Duong, Y. Yin, H.T. Pham, D. Walter, J. Peng, Y. Wu, L. Li, H. Shen, N. Wu, N. Mozaffari, G. Andersson, K.R. Catchpole, K.J. Weber, T.P. White, *Adv. Funct. Mater.* **2020,***30*, 1907962.
[243] C. Chen, S. Zhang, S. Wu, W. Zhang, H. Zhu, Z. Xiong, Y. Zhang, W. Chen, *RSC Adv.* **2017,***7*, 35819.
[244] N.-G. Park, M. Grätzel, T. Miyasaka, K. Zhu, K. Emery, *Nat. Energy* **2016,***1*, 16152.

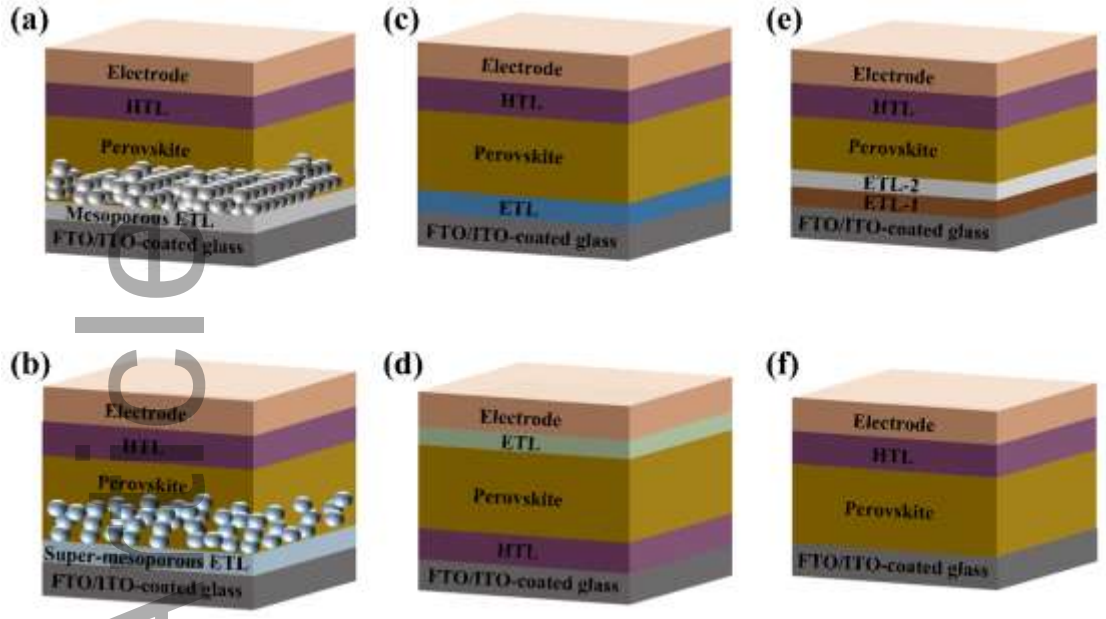

Figure 1. Schematic diagram of device structure: (a) mesoporous, (b) super-mesoporous, (c) planar n-i-p (regular), (d) planar p-i-n (inverted), (e) bi-layer, and (f) ETL-free.

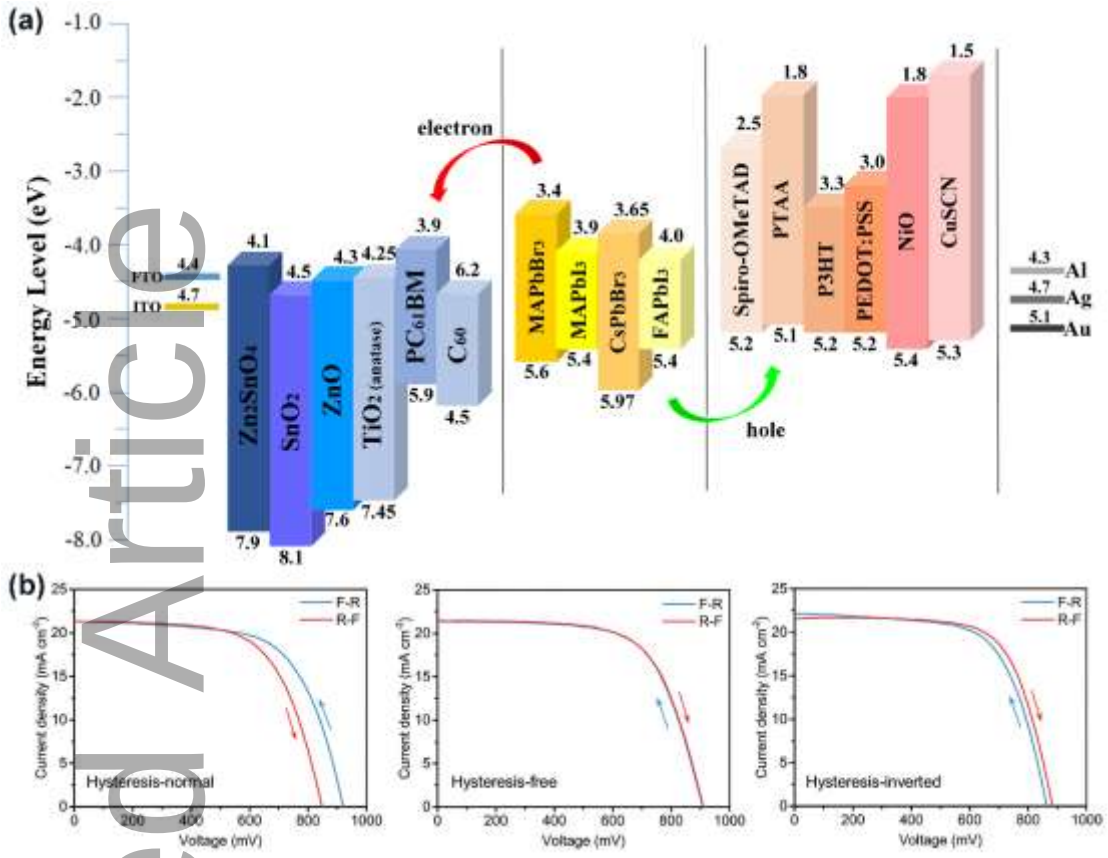

Figure 2. (a) Schematic diagram of energy levels of typical materials in PSCs. (b) Different types of hysteresis in PSCs. Reproduced with permission.[39] Copyright 2017, The Royal Society of Chemistry.

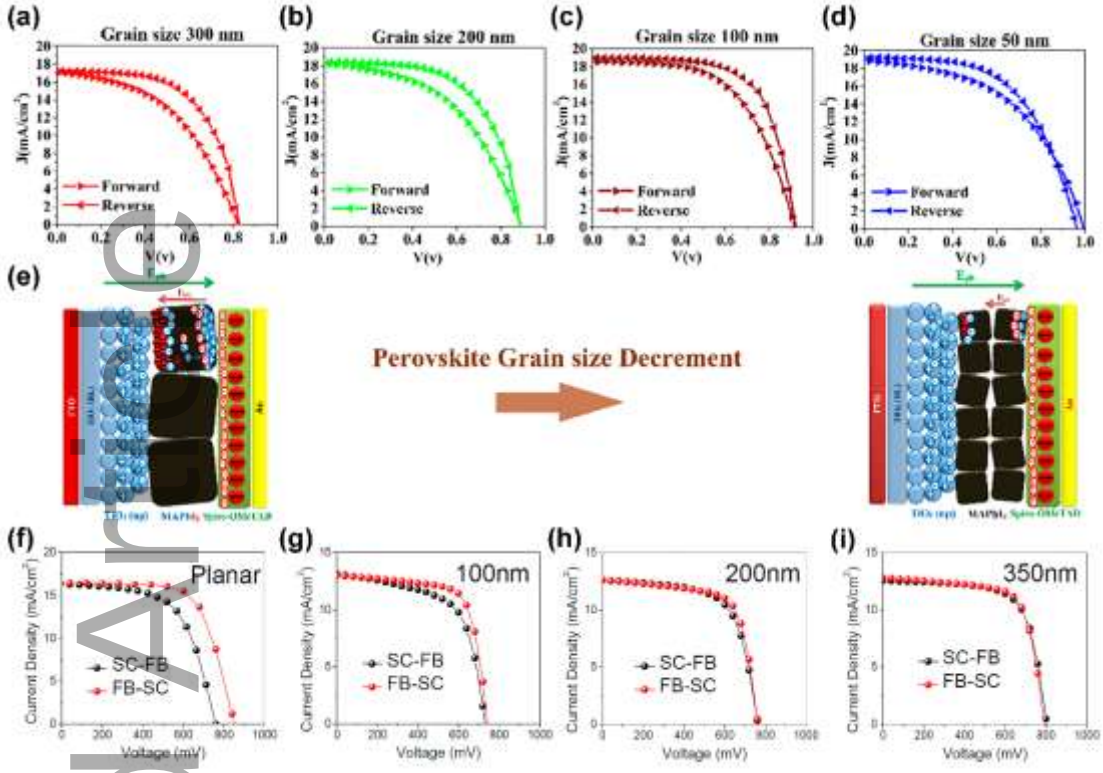

Figure 3.*J-V*curve for the fabricated PSCs with different perovskite grain sizes: (a) 300 nm;(b) 200 nm;(c) 100 nm; and (d) 50 nm. (e) The difference in ion migration in various perovskite grain sizes. Reproduced with permission.[46] Copyright 2016, American Chemical Society Publications. The *J-V* curve for PSCs employed mesoporous TiO_2 with different thickness: (f) 0 nm (planar); (g) 100 nm; (h) 200 nm; (i) 350 nm. Reproduced with permission.[49] Copyright 2015, American Chemical Society Publications.

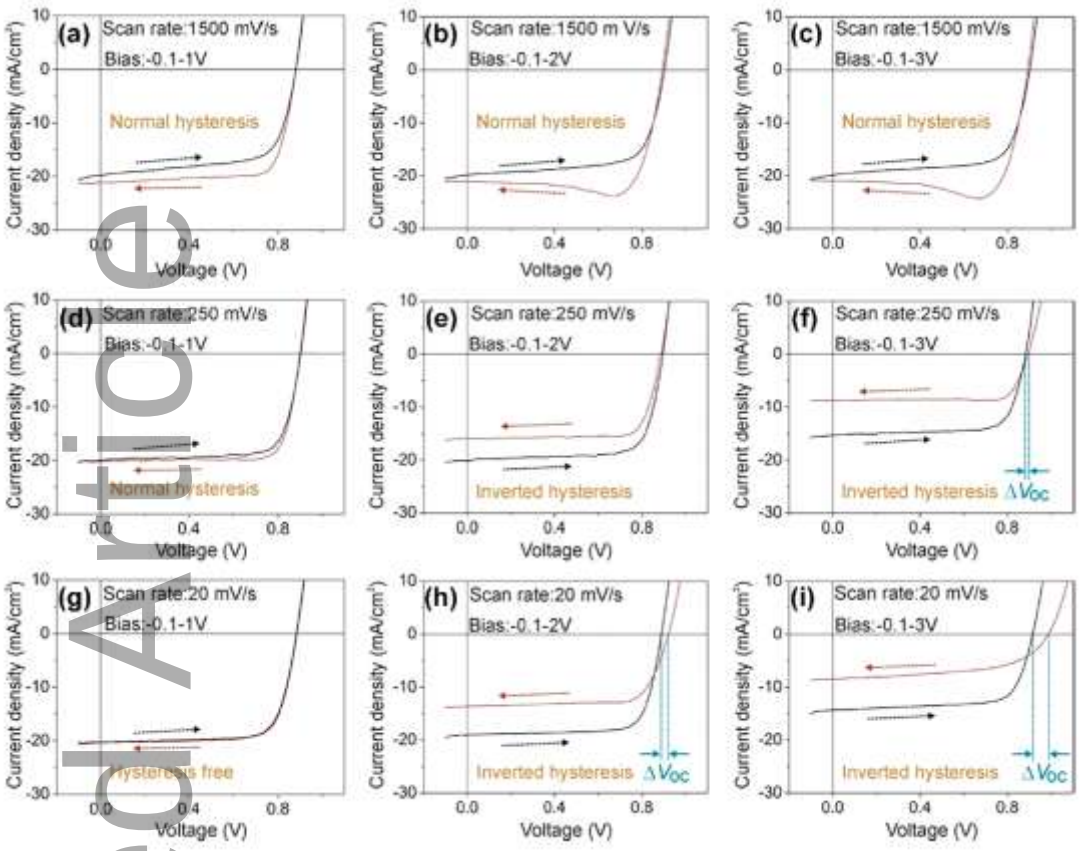

Figure 4. The effect of bias voltage and scan rate on hysteresis. Reproduced with permission.[64] Copyright 2018, American Chemical Society Publications.

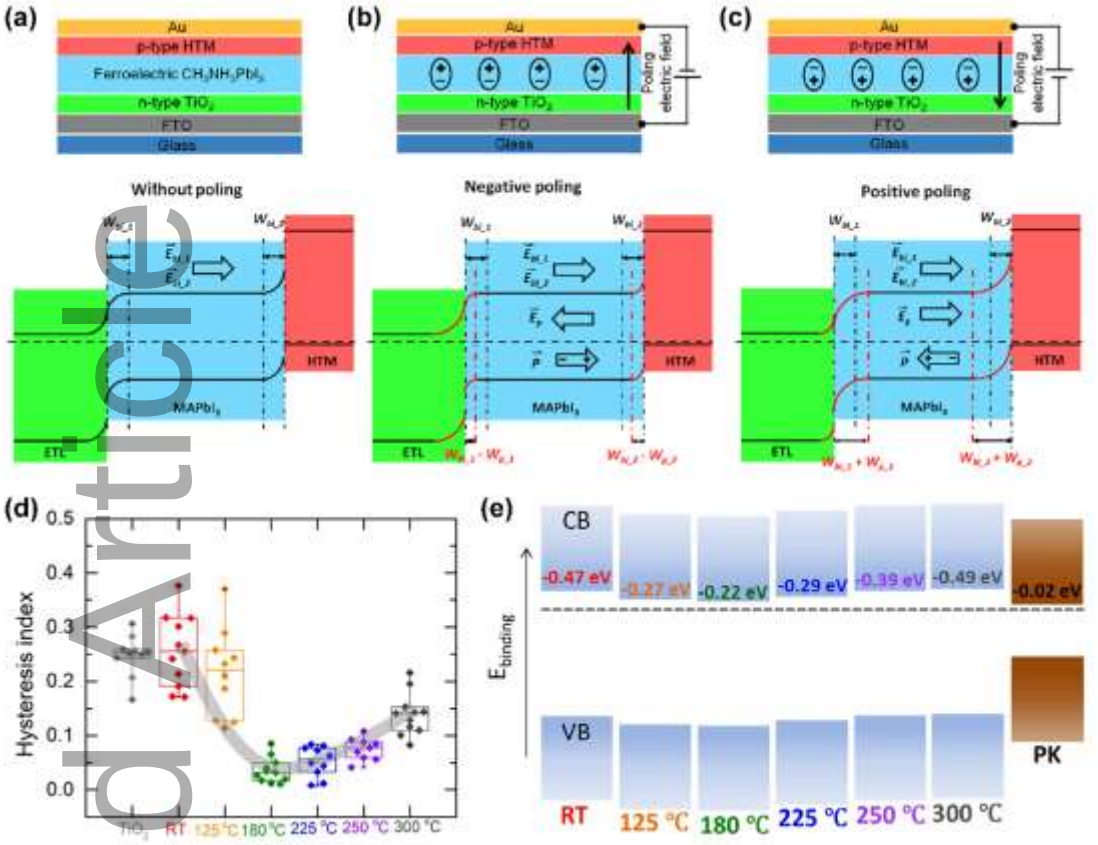

Figure 5. Schematic and band diagram of planar n-i-p PSCs under different poling conditions: (a) without poling, (b) negative poling, and (c) positive poling.E_{bi-1} and E_{bi-2} represent the built-in electric field in the perovskite layer near the ETL side and HTL side, respectively. W_{bi-1} and W_{bi-2} represent the width of the depletion region near the ETL side and HTL side, respectively. W_{p-1} and W_{p-2} represent the width of the depletion region caused by ferroelectric polarization in the perovskite layer near ETL side and HTL side, respectively. And P represents the ferroelectric polarization. Reproduced with permission.[81] Copyright 2015, Elsevier Inc Publications. (d) The relationship between the annealing temperature of the SnO_x ETL and the *HI*. (e) Schematic diagram of the energy bands of the ETL and perovskite. Dashed black line represents the Fermi level.Reproduced with permission.[88] Copyright 2018, American Chemical Society Publications.

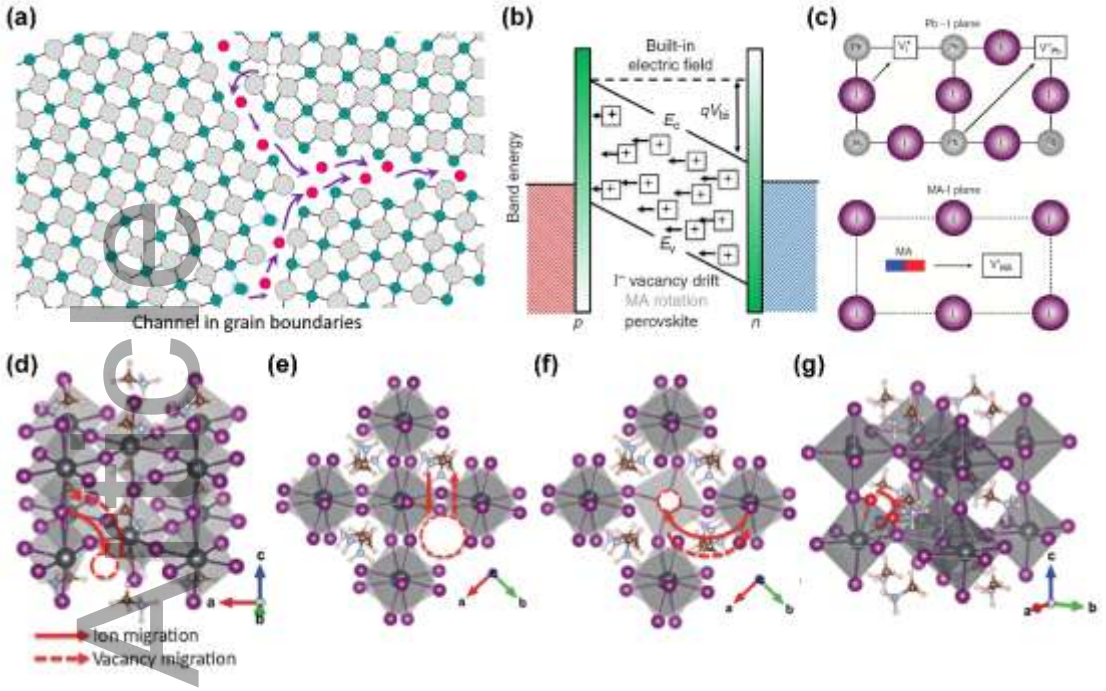

Figure 6. (a) Illustration of the ion migration pathways enabled by open space and wrong bonds at GBs.Reproduced with permission.[91] Copyright 2016, American Chemical Society Publications. (b) Schematic illustration of I^-vacancy migration and its influence on the electric field. (c) Schematic illustration of the three ion migration mechanisms involving between neighbouring positions: I^- migration along an octahedron edge; Pb^{2+} migration along the diagonal direction <110>; MA^+ migration into a neighbouringvacant A-site cage involving motion normal to the unit cell face composed of four iodide ions. Reproduced with permission.[100] Copyright 2015, Nature Publishing Group. Diffusion pathways for the (d) V_I, (e) V_{MA}, (f) V_{Pb} and (g) I_i defects.For I_i, the initial and the final configurations are shown. Vacancies are highlighted with dashed circles. Reproduced with permission.[101] Copyright 2015, The Royal Society of Chemistry.

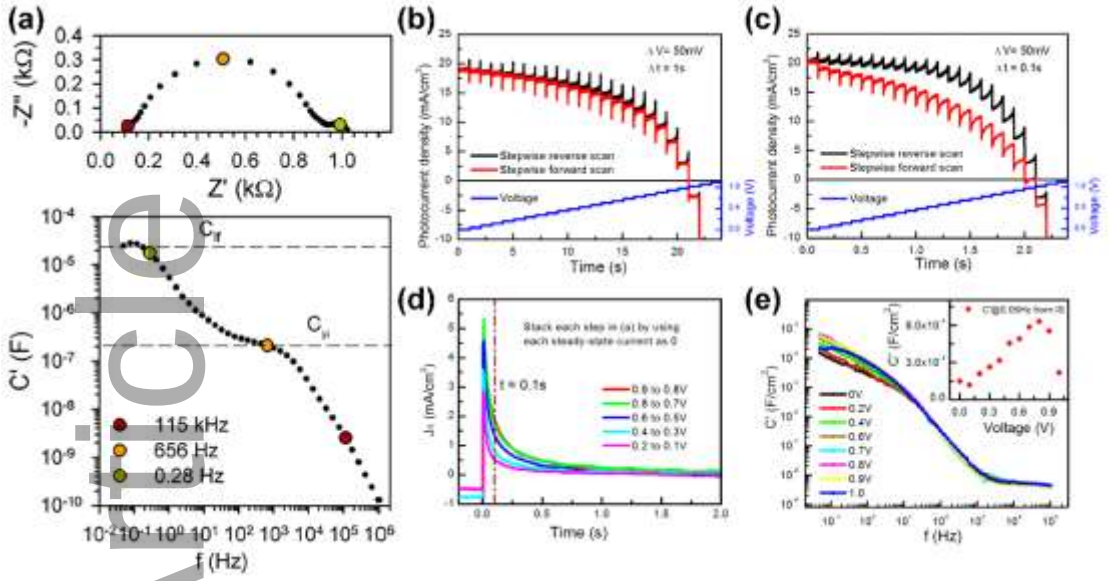

Figure 7. (a)Complex impedance plot (imaginary part of the impedance, Z″, versus the real part, Z′) and Bode plot of the real part of the capacitance, C′, obtained under dark conditions at 0.9 V applied DC bias (bottom image).Reproduced with permission.[107] Copyright 2014, American Chemical Society Publications. Time-dependent photocurrent response under reverse and forward stepwise scans with (b) 1 s step time and (c) 0.1 s step time. (d) Decay of dynamic non-steady-state photocurrent Jn(t) with time during stepwise reverse scan. (e) Capacitance (C′, real part) as a function of frequency at different bias under illumination; the inset is the relation of C′ with applied bias obtained from IS measurement at 0.05 Hz. Reproduced with permission.[105] Copyright 2015, American Chemical Society Publications.

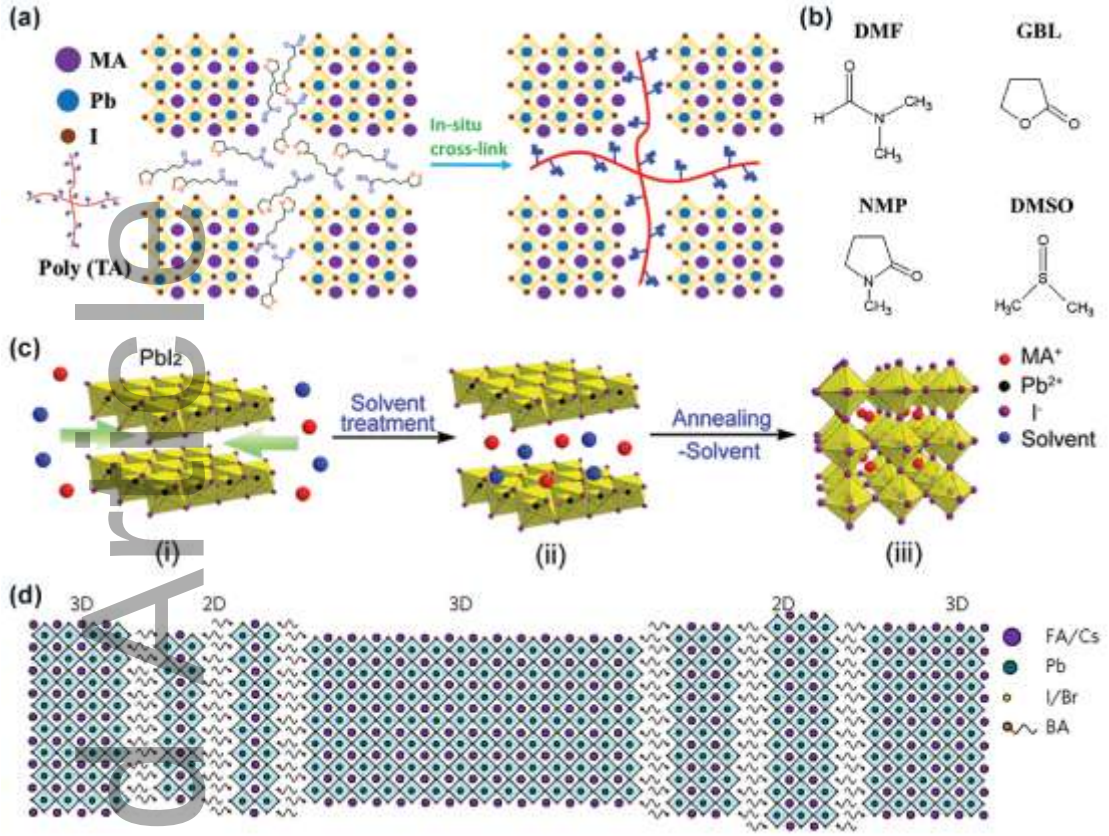

Figure 8.(a) Working mechanism of crystal modification and trap passivation for Poly(TA) in PSCs. Reproduced with permission.[122] Copyright 2020, Wiley-VCH Publications. (b) Molecular structure of DMF, GBL, NMP, and DMSO.Reproduced with permission.[129] Copyright 2017, Elsevier Inc Publications. (c) Scheme of the $MAPbI_3$ perovskite thin film forming process. (i) PbI_2 and MAI in the mixture solvent of DMF and DMSO; (ii) exfoliation and intermediate phase formation after solvent treatment; (iii) $MAPbI_3$ perovskite thin film forms after thermal annealing. Reproduced with permission.[130] Copyright 2015, The Royal Society of Chemistry. (d) Schematic illustration of the self-assembled 2D-3D perovskite film structure. Reproduced with permission.[145] Copyright 2017, Nature Publishing Group.

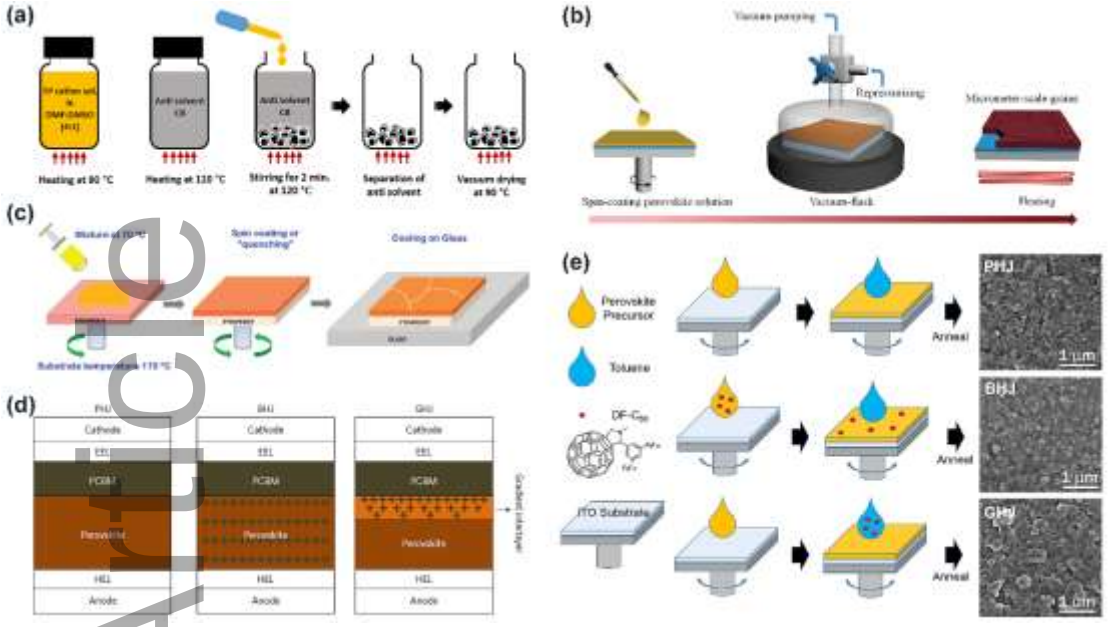

Figure 9. (a) Schematic diagram for the preparation of triple-cation perovskite powder. Reproduced with permission.[149] Copyright 2019, American Chemical Society Publications. (b) Schematic illustration of formation of perovskite film via vacuum flash-assisted solution processing(VASP). Reproduced with permission.[150] Copyright 2016, Science Publishing Group. (c) Hot-casting scheme for crystal growth. Reproduced with permission.[154] Copyright 2015, Science Publishing Group. (d) Schematic diagram of three types of inverted PSCs with heterojunction structures.The interlayer in GHJ is composed of perovskite with a gradient distribution of PCBM. Reproduced with permission.[156] Copyright 2016, Nature Publishing Group.(e) Fabrication process and SEM image of perovskite films with PHJ, BHJ and GHJ structure. Reproduced with permission.[162] Copyright 2017, American Chemical Society Publications.

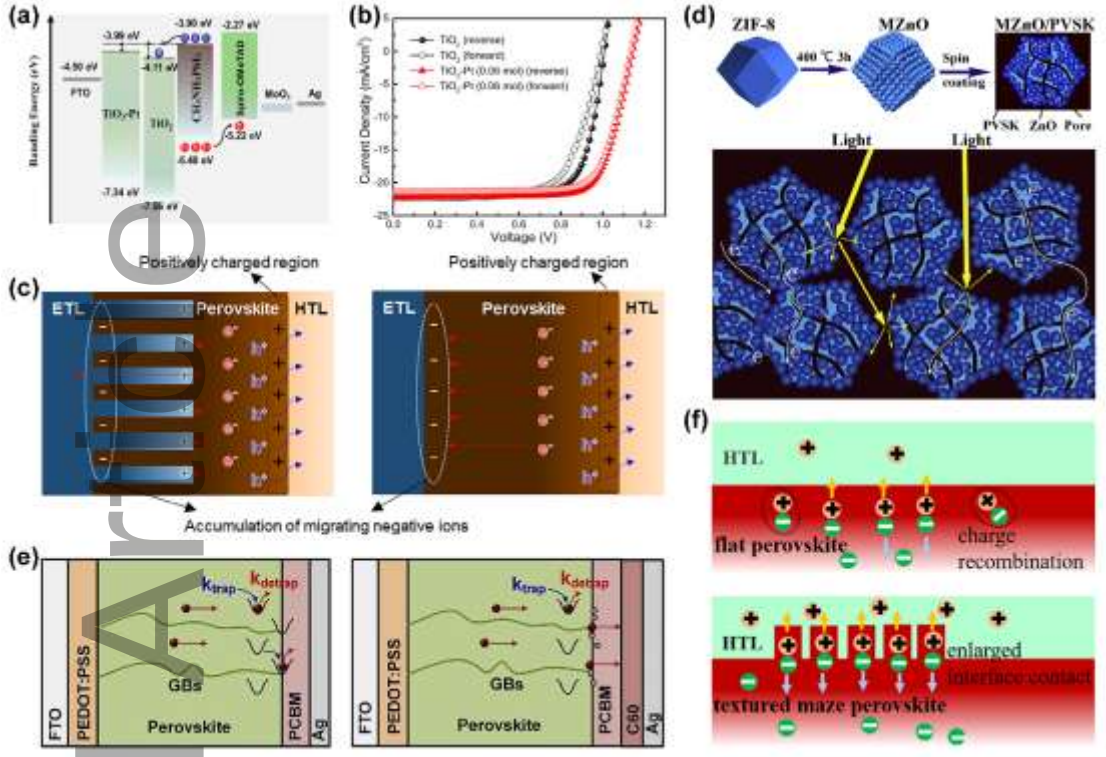

Figure 10. (a) The energy level diagram of PSCs based on TiO_2 or TiO_2-Pt ETLs. (b) *J-V* curve under both FS and RS. Reproduced with permission.[168] Copyright 2018, Wiley-VCH Publications.(c) Schematic of charge accumulation and carrier extraction in TiO_2 nanorods and planar TiO_2 based PSCs. Reproduced with permission.[173] Copyright 2018, Elsevier Inc Publications. (d) Schematic diagrams of formation of MOF-Derived ZnO Polyhedra and their use as ETLs to enhance light harvesting and electrons extraction. Reproduced with permission.[196] Copyright 2020, Elsevier Inc Publications. (e) The charge transfer mechanism of perovskites with $PC_{61}BM$ and $PC_{61}BM/C_{60}$ layers. Reproduced with permission.[54] Copyright 2018, Elsevier Inc Publications. (f) Schematic illustration of the insufficient charge separation at the flat perovskite/HTL interface in the absence of ETL (top image) and the facilitated hole extraction at maze-like perovskite/HTM interface induced by enlarged interfacial contact (bottom image). Reproduced with permission.[203] Copyright 2019, Wiley-VCH Publications.

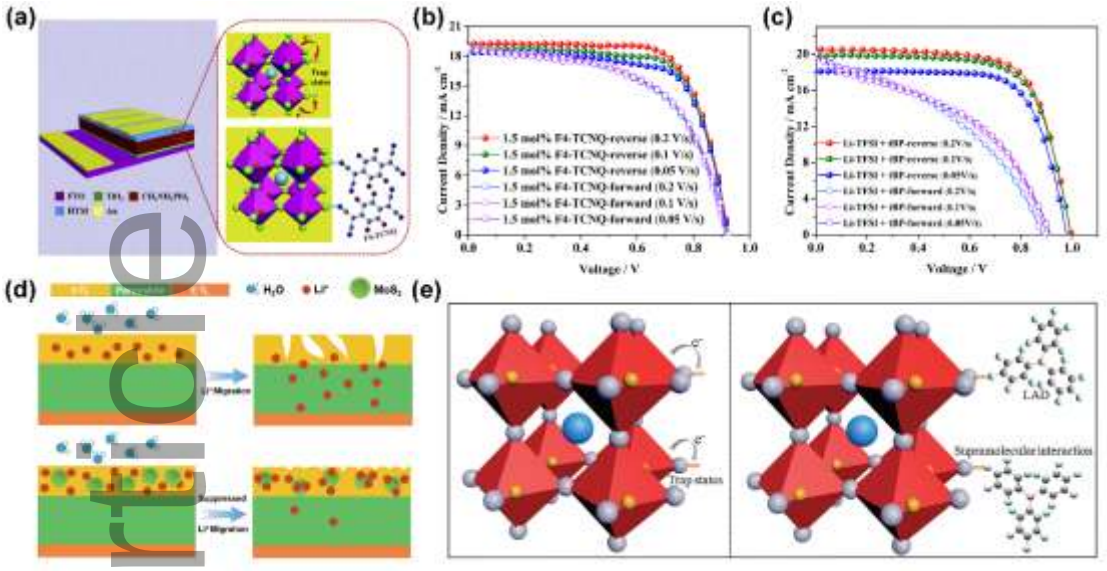

Figure 11. (a) Possible trap states caused by surface iodine ions and passivation mechanism with F4-TCNQ. *J-V* curves of devices based on (b) 1.5 mol% F4-TCNQ or (c) Li-TFSI, tBP doped Spiro-OMeTAD measured at FS and RS with different scan rate: 0.05, 0.1 and 0.2 V s^{-1}. Reproduced with permission.[209] Copyright 2017, Elsevier Inc Publications. (d) A schematic of the adsorbent function of flower-like MoS_2 nanoparticles for Li^+ ions in the Spiro-OMeTAD layer and suppressed Li^+ migration from the Spiro-OMeTAD layer to the perovskite layer.Reproduced with permission.[207] Copyright 2019, The Royal Society of Chemistry. (e) Schematic of the mechanism for LAD surface passivation. Reproduced with permission.[226] Copyright 2018, The Royal Society of Chemistry.

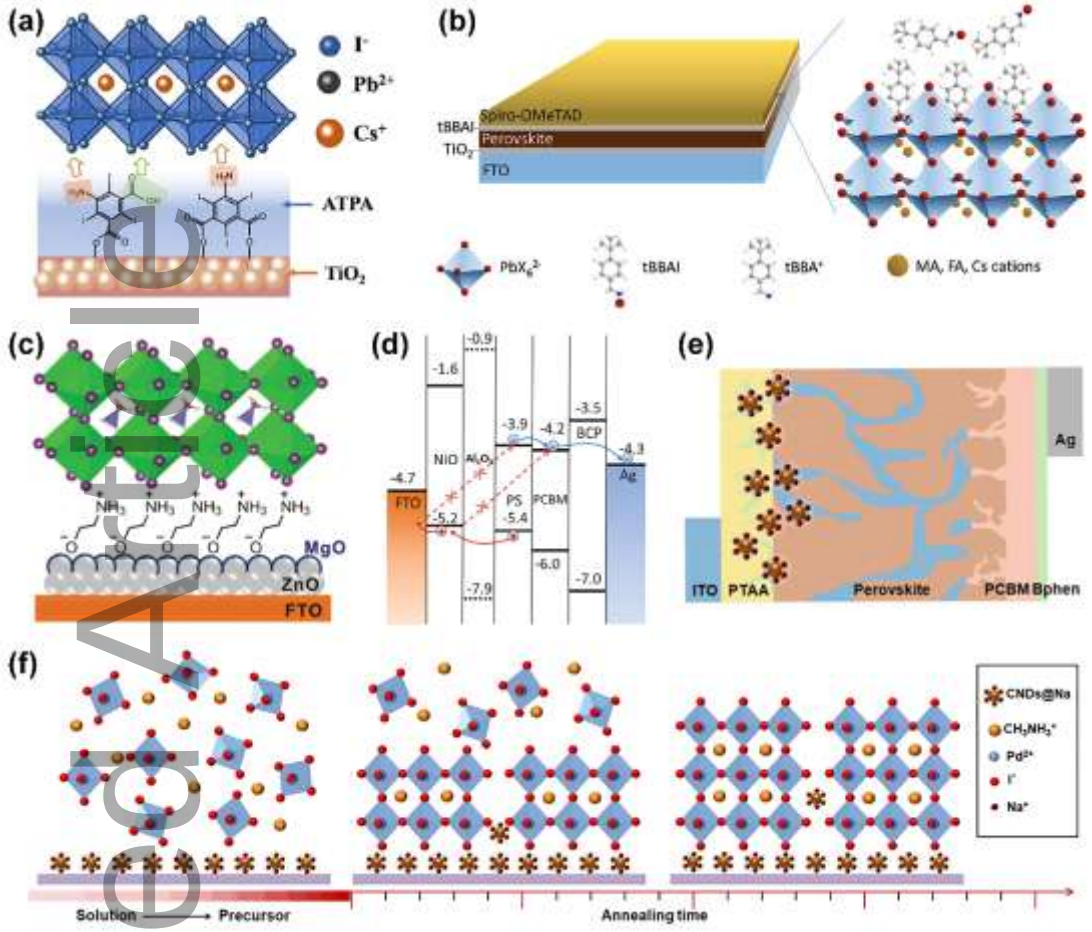

Figure 12. (a) Schematic illustration of the formation of ATPA on the TiO_2 layer. Reproduced with permission.[229] Copyright 2020, Wiley-VCH Publications. (b) Structures of a tBBAI-passivated PSCs. Reproduced with permission.[234] Copyright 2020, Wiley-VCH Publications. (c) Schematic illustration of a planar PSCs device modified with ZnO–MgO–EA^+.Reproduced with permission.[237] Copyright 2018, Wiley-VCH Publications. (d) The cell energy level (versusvacuum) diagram highlighting the dual blocking effect of the hybrid "compact NiO/meso-Al_2O_3" interfacial layer. Reproduced with permission.[239] Copyright 2018, The Royal Society of Chemistry. (e) Schematic for CNDs@Na passivated interfacial traps of the PSCs. (f) Molecular dynamics of perovskite on CNDs@Na-coated PTAA. Reproduced with permission.[240] Copyright 2020, Wiley-VCH Publications.

Table 1. Comparison of the *HI* values and photovoltaic performance of PSCs with planar and mesoporous structures.

No.	Cell structure	Photovoltaic performance				Scan direction	HI	Ref.
		V_{OC} (V)	J_{SC} (mA cm^{-2})	FF	PCE (%)			
1	FTO/c-TiO_2/mp-TiO_2/$MAPbI_3$/Spiro-OMeTAD/Au	0.935	18.0	0.68	11.4	FS	0.055	[50]
		0.950	17.9	0.72	12.2	RS		
	FTO/c-TiO_2/ $MAPbI_3$/Spiro-OMeTAD/Au	0.892	17.1	0.41	6.3	FS	0.362	
		0.932	17.1	0.64	10.2	RS		
2	FTO/Mg-dopedquantum dots SnO_2/mp-SnO_2/$MAPbI_3$/ Spiro-OMeTAD/Au	1.112	22.80	0.7574	19.21	FS	-0.0005 [a]	[20]
		1.112	22.80	0.7578	19.20	RS		
	FTO/Mg-dopedquantum dots SnO_2/ $MAPbI_3$/ Spiro-OMeTAD/Au	1.082	21.48	0.7349	17.08	FS	0.0437 [a]	
		1.111	21.67	0.7421	17.86	RS		
3	FTO/c-TiO_2/mp-TiO_2/$MAPbI_3$/Spiro-OMeTAD/Ag	-	-	-	-	FS	0.06	[49]
		-	-	-	-	RS		
	FTO/c-TiO_2/$MAPbI_3$/Spiro-OMeTAD/ Ag	-	-	-	-	FS	0.23	
		-	-	-	-	RS		
4	FTO/c-TiO_2/ultrathin mp-TiO_2/$MAPb(I_{0.965}Cl_{0.035})_3$/ Spiro-OMeTAD/Au	1.06	22.81	0.73	17.7	FS	0.045	[60]
		1.07	22.82	0.76	18.5	RS		
	FTO/c-TiO_2/$MAPb(I_{0.965}Cl_{0.035})_3$/Spiro-OMeTAD/Au	1.04	22.38	0.70	16.3	FS	0.067	
		1.05	22.45	0.74	17.4	RS		
5	FTO/c-TiO_2/m-TiO_2/$MAPbI_3$/Carbon	0.95	17.94	0.45	7.69	FS	0.3237 [a]	[61]
		1.01	17.74	0.64	11.37	RS		
	FTO/c-TiO_2/ $MAPbI_3$/Carbon	0.81	12.42	0.20	2.01	FS	0.6186 [a]	
		0.97	12.72	0.43	5.27	RS		
6	FTO/c-TiO_2/mp-TiO_2/$MAPbI_3$/Spiro-OMeTAD/Carbon	0.826	9.77	0.46	3.73	FS	0.181	[37]
		0.847	10.01	0.58	4.93	RS		

7	FTO/c-TiO_2/ $MAPbI_3$/Spiro-OMeTAD/Carbon	0.866	3.21	0.11	0.31	FS	0.611	[36]
		0.918	3.01	0.37	1.03	RS		
	FTO/planar SnO_2 nanorods/mesoporous BF_4^--capped SnO_2 emulsified microspheres/$Cs_{0.05}(MA_{0.15}FA_{0.85})_{0.95}Pb(I_{0.85}Br_{0.15})_3$/Spiro-OMeTAD/Au	1.140	23.18	78.15	20.65	FS	0.033	
		1.156	23.45	78.77	21.35	RS		
	FTO/planar SnO_2 nanorods/$Cs_{0.05}(MA_{0.15}FA_{0.85})_{0.95}Pb(I_{0.85}Br_{0.15})_3$/Spiro-OMeTAD/Au	1.108	22.52	0.724	18.07	FS	0.051	
		1.128	22.45	0.752	19.04	RS		

[a)]The HI is calculated according to **Equation 2** when the references does not give it.

Table 2. The performance of PSC obtained by TiO_2 ETL with various elements doping.

No.	Cell structure	Doped ion	Photovoltaic performance				Scan direction	HI	Ref.
			V_{OC} (V)	J_{SC} (mA cm^{-2})	FF	PCE (%)			
1	FTO/c-TiO_2/Li-doped mp-TiO_2/$MAPbI_3$/PTAA/Au	Li	1.01	22.32	0.765	17.25	FS	0.001 a)	[165]
			1.02	22.11	0.766	17.27	RS		
2	FTO/ Ta-doped c-TiO_2/mp-TiO_2/$MAPbI_3$/Spiro-OMeTAD/Ag	Ta	1.00	19.05	0.70	13.29	FS	0.078 a)	[166]
			1.03	19.21	0.73	14.41	RS		
3	FTO/ Nb-doped c-TiO_2/mp-TiO_2/$MAPbI_3$/Spiro-OMeTAD/Ag	Nb	1.00	19.12	0.68	12.96	FS	0.093 a)	[166]
			1.02	19.26	0.73	14.29	RS		
4	FTO/Nb-doped c-TiO_2/$MAPbI_3$/Spiro-OMeTAD/Au	Nb	1.04	22.80	0.6434	15.19	FS	0.023	[167]
			1.05	22.90	0.6696	16.12	RS		
5	FTO/Pt-doped c-TiO_2/$MAPbI_3$/Spiro-OMeTAD/MoO_3/Ag	Pt	1.13	22.43	0.74	19.03	FS	0.006 a)	[168]
			1.14	22.26	0.75	19.15	RS		
6	FTO/Ru-doped c-TiO_2/mp-TiO_2/$MAPbI_3$/Spiro-OMeTAD/ Au	Ru	1.05	23.51	0.70	17.34	FS	0.056 a)	[169]
			1.11	23.51	0.70	18.35	RS		
7	FTO/Co-doped c-TiO_2/ $[CsPbI_3]_{0.05}[(FAPbI_3)_{0.85}(MAPbBr_3)_{0.15}]_{0.95}$/Spiro-OMeTAD/Au	Co	1.143	21.04	0.756	18.17	FS	0.025	[170]
			1.165	21.08	0.778	19.10	RS		
8	FTO/c-TiO_2/Ru-doped mp-TiO_2/ $(FAPbI_3)_{0.85}(MAPbBr_3)_{0.15}$/PTAA/Au	Ru	1.126	22.50	0.7520	18.65	FS	0.015 5	[172]
			1.128	22.55	0.7655	18.94	RS		

a) The HI is calculated according to **Equation 2** when the references does not give it.

TOC

Current density-voltage (J-V) hysteresis in perovskite solar cells (PSCs) is a major challenge in this field.This review mainly focuses on the possible origins and

factors of J-V hysteresis behavior in PSCs and summarize the strategies to suppress the hysteresis. Finally, we also provide insights on the future development of the J-V hysteresis in PSCs.